Geological Society of America Bulletin

Magmatic history of Dabbahu, a composite volcano in the Afar Rift, Ethiopia

L. Field, J. Blundy, A. Calvert and G. Yirgu

Geological Society of America Bulletin 2013;125, no. 1-2;128-147
doi: 10.1130/B30560.1

Notes

Magmatic history of Dabbahu, a composite volcano in the Afar Rift, Ethiopia

L. Field[1,†], J. Blundy[1], A. Calvert[2], and G. Yirgu[3]
[1]*School of Earth Sciences, University of Bristol, Wills Memorial Building, Queen's Road, Bristol BS8 1RJ, UK*
[2]*U.S. Geological Survey, 345 Middlefield Road, MS-937, Menlo Park, California 94025, USA*
[3]*Department of Earth Sciences, University of Addis Ababa, Addis Ababa, Ethiopia*

ABSTRACT

Dabbahu is a composite volcano at the north end of the active Manda-Hararo segment of the Afar Rift in northern Ethiopia. We present 93 new whole-rock analyses, mineral analyses from 65 samples, and 9 new ^{40}Ar-^{39}Ar dates for rocks ranging in composition from mildly alkaline basalt through trachyandesite to peralkaline rhyolite (comendite and pantellerite) erupted from Dabbahu. These data, supplemented by a new geological map, are used to provide insights into the evolution of the volcano. We show that Dabbahu has been active for over 67 k.y., but an apparent hiatus occurred between the eruption of comendite (29 ka) and pantellerite (ca. 8 ka) lavas. Mineral data for olivine, clinopyroxene, plagioclase, and alkali feldspar show a remarkably extensive range of solid solution across the rock suite consistent with protracted fractionation from basalt to rhyolite. The parental basalt is compositionally similar to recent rift-related basalts in the Manda-Hararo rift, with low initial H_2O contents (<1 wt%). Closed-system fractionation increased H_2O contents of residual liquids sufficiently for some rhyolites to erupt both explosively and effusively. The diverse magma types were erupted from a relatively closely spaced network of vents and fissures. Field evidence indicates that magmas were not erupted in a simple fractionation sequence. Some mixing occurred between magmas of less-evolved compositions and more-evolved compositions shortly prior to, or during, eruption. The differentiation of basalt to rhyolite must have occurred on time scales that were relatively short compared to the lifetime of the volcano, probably due to the small volumes of basalt intruded into the crust and consequently enhanced cooling and crystallization rates. A network of stacked sills or closely spaced dikes in the shallow to midcrust represents the most plausible configuration of the subvolcanic plumbing system. Input of new magma batches into such a system may serve as a key eruption trigger at Dabbahu.

INTRODUCTION

The Ethiopian rift system is one of the few locations worldwide where active continental breakup can be observed (e.g., Hayward and Ebinger, 1996). The current phase of rifting began in September 2005 with a major 60 km basaltic-dike intrusion and a small rhyolitic eruption, believed to be the first such eruption in ~150 yr; just seven of Africa's volcanoes have erupted in historical times (Ayele et al., 2007). The Afar region now forms a triangular low-lying region (–120–500 m elevation) where the Red Sea, the Gulf of Aden, and the Ethiopian portion of the East African Rift meet (Fig. 1A). It is bordered by the Ethiopian plateau to the west (~2000–3000 m elevation), the Somali plateau to the southeast, and the Danakil block to the northeast. As early as 1970, it was suggested that the Afar Depression was formed by the separation of Arabia away from the African and Somalian plates (McKenzie et al., 1970), which has occurred over the past ~30 m.y. (Wolfenden et al., 2005). The Arabian plate is currently moving away from Africa at a rate of 16 mm yr^{-1}, and across the northern sector of the Main Ethiopian Rift, recent studies suggest that there is 3–6 mm yr^{-1} of movement between the Somalia and African plates (Chu and Gordon, 1998, 1999). In the Gulf of Aden, rifting has progressed to oceanic spreading (e.g., Manighetti et al., 1997). Similarly, the Red Sea rift has opened southward as far as 14°N (Prodehl et al., 1997), where it is believed to have moved on land, thus isolating the Danakil microplate.

The locus of strain has shifted southward from the Red Sea rift to subaerial northern Afar (Fig. 1A) in a succession of discrete rift jumps; most volcanic and tectonic activity in Afar is associated with this on-land continuation of the Red Sea rift (Acocella et al., 2008). As the rift became localized at ca. 3 Ma, magmatism and faulting in Afar became focused along ~60-km-long segments (Hayward and Ebinger, 1996), which are zones of fissural basalt lava flows, aligned basaltic scoria cones, volcanic edifices, shallow seismicity, positive gravity anomalies, collapsed grabens, and domino-tilted blocks (Acocella, 2010; Barberi and Varet, 1977; Beutel et al., 2010; Ebinger et al., 2010; Hayward and Ebinger, 1996). These magmatic segments are the locus of magma intrusion and formation of new crust. The individual rift segments are similar in size, morphology, structure, and spacing to those observed along an oceanic boundary (e.g., Hayward and Ebinger, 1996). To the north, the segments of Erta'Ale and Tat'Ale are characterized by axial volcanic ridges of transitional alkali-tholeiitic basalt composition (Barberi et al., 1972). Southward continuation of the rift steps across to the western Alayta segment, and then to the Manda-Hararo rift segment, which consists of the active northern Dabbahu magmatic segment and the currently tectonically inactive southern Hararo segment (Rowland et al., 2007). Since 2005, the Dabbahu magmatic segment has been subject to considerable scientific scrutiny using a combination of ground-based and satellite geodesy, potential field measurements, seismology, and petrology. Over this time period, a series of rifting events has led to the emplacement of 13 basaltic dikes with a total width in excess of 8 m (Hamling et al., 2009, 2010). Three eruptions have occurred in this region since 2005: a rhyolitic ash eruption following the 2005 diking event at Da'Ure on the northern flanks of Dabbahu (Wright et al., 2006), and two basaltic-fissure eruptions in the Dabbahu magmatic segment ~30 km south of Dabbahu (Ferguson et al., 2010).

†E-mail: l.p.field@gmail.com

GSA Bulletin; January/February 2013; v. 125; no. 1/2; p. 128–147; doi: 10.1130/B30560.1; 10 figures; 2 tables; Data Repository item 2012337.

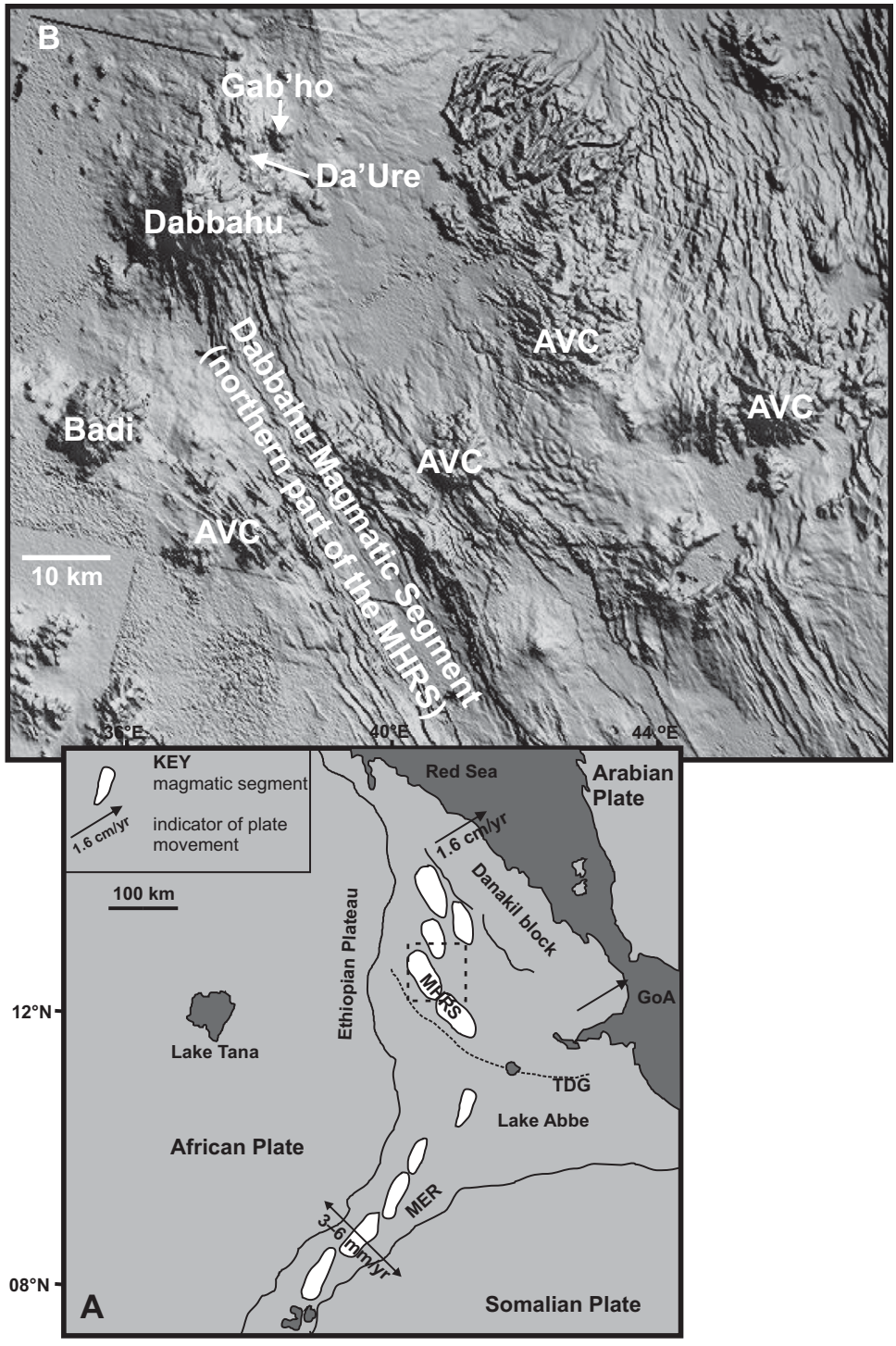

Figure 1. Location of study area in the Afar region of Ethiopia. (A) Sketch map showing the regional setting of Afar after Rowland et al. (2007). Plate movement rates are from Chu and Gordon (1998, 1999). MER—Main Ethiopian Rift, MHRS—Manda-Hararo rift segment, TDG—Tendaho-Goba'ad discontinuity, GoA—Gulf of Aden. Dashed line box indicates approximate area of location of study area. (B) Detail of the Dabbahu magmatic segment (northern end of the Manda-Hararo rift segment), AVC—Ado Ale volcanic complex. Image is derived from Spot digital elevation model (courtesy of Sophie Hautot).

The Afar Rift is punctuated by a series of composite volcanoes that have eruption products ranging from basalt to rhyolite via a range of intermediate magma types. Although the exact relationship of these volcanic centers to the main rift-related basaltic magmatism remains unclear, there is general consensus that intracrustal differentiation of rift basalts played a key role in generating the evolved magmas. Here, we focus on one of the composite volcanoes, Dabbahu, at the northern end of the Manda-Hararo rift segment, using a combination of geochemistry, geochronology, and petrology to constrain the processes and timing of differentiation in order to place the magmatism in the wider context of rift-related activity.

GEOLOGICAL SETTING

Dabbahu, also known as Boina, Boyna, or Moyna, is a Quaternary volcano situated at the northern end of the Manda-Hararo rift segment (12°35′00″N, 40°28′00″E; Fig. 1B). The Manda-Hararo rift segment is characterized by a 35-km-wide central depression punctuated

by silicic edifices (Lahitte et al., 2003a). The northern part of the Manda-Hararo rift segment, known as the Dabbahu magmatic segment, is an area ~60 km long and ~15 km wide trending SSE-NNW from a dissected central silicic complex known as the Ado'Ale volcanic complex (Fig. 1B) to Dabbahu (Rowland et al., 2007). Dabbahu was first sketch-mapped by Brinckmann and Kuersten (1970) from aerial photographs, and subsequently by Barberi et al. (1974b) following field expeditions. Barberi et al. (1974a, 1974b) described Dabbahu as an ~1400-m-high volcanic edifice, rising from a base of fissural basalts at an elevation of ~350 m above sea level. The total erupted volume of the edifice is in excess of 115 km^3; accurately estimating the erupted volume of the Dabbahu lavas is problematic because their full extent has not yet been fully defined due to difficulties in accessing all areas of the volcano, particularly the eastern side, which remains unsampled. Dabbahu is widely cited as an example of a full fractional crystallization sequence from mildly alkaline basalts to mildly peralkaline rhyolites, erupted from a central volcano above a shallow magma chamber (Barberi et al., 1974b, 1974c; Bizouard et al., 1980). Since the pioneering work of the Consiglio Nazionale delle Ricerche and Centre National de la Recherché Scientifique (CNR-CNRS) campaigns (Barberi et al., 1974b, 1974c; Bizouard et al., 1980), no further analysis has been carried out, due in no small part to the remoteness and inaccessibility of the area. Interest in the volcano was reawakened in 2005 when a small rhyolitic ash eruption and extrusion of a small pumice dome from the Da'Ure vent on the northern flanks of Dabbahu (12°39′00″N, 40°31′10″E) coincided with the largest dike opening event ever measured (Ayele et al., 2007). Modeled as a basaltic dike injection, ~10 km deep, it was shown that over 8 m of opening occurred along a distance of ~60 km. This event may have triggered the Da'Ure eruption by interaction of basaltic magma with a shallow silicic reservoir (Wright et al., 2006).

SAMPLING AND ANALYTICAL TECHNIQUES

Field work and collection of over 100 samples were undertaken during field campaigns in 2008 and 2009. Aerial photographs were obtained as part of airborne light detection and ranging (LiDAR) acquisition by the Natural Environment Research Council of the UK Airborne Research and Survey Facility (NERC ARSF). Whole-rock major elements were analyzed by X-ray fluorescence (XRF) in 94 samples; trace-element data for the same samples will be presented elsewhere. Thin sections of these samples were assessed using a scanning electron microscope (SEM) before major-element analysis of individual minerals and glasses by electron microprobe (EMP). Sixty-eight samples were manually point counted to ascertain the fraction of phenocrysts. Samples for ^{40}Ar-^{39}Ar dating were collected during the field campaign of 2008, and nine samples were chosen to give as wide a compositional, stratigraphic, and spatial spread across Dabbahu as possible. Full details of all analytical techniques used are provided in the supplementary documentation.[1]

COMPOSITIONAL OVERVIEW

In terms of the total alkalis–silica diagram (Le Maitre, 2002), Dabbahu shows a complete sequence of rock types from basalt through to rhyolite (Fig. 2). Silica content (on an anhydrous basis) ranges between 45.6 wt% SiO_2 (sample 101a, a basaltic scoria cone) and 74.0 wt% SiO_2 (sample 071, a comenditic obsidian). From a chemical viewpoint, the basalts are transitional in character, closely following the alkaline-subalkaline divide of Irvine and Baragar (1971). They are more alkaline than the light rare earth element (LREE)–depleted basalts of the Manda-Hararo rift segment (Barrat et al., 2003). There are apparent slight compositional gaps between 56 and 59 wt% SiO_2, and between 64 and 69 wt% SiO_2. The peralkalinity of the rhyolites and trachytes was calculated as NK/A = molar $[Na_2O + K_2O]/Al_2O_3$ >1 (e.g., Macdonald, 1974; Macdonald and Bailey, 1973), and the peralkaline rhyolites were further subdivided as comenditic or pantelleritic using the criteria of Macdonald (1974), whereby pantellerites contain higher Fe and lower Al than comendites. Fifty-seven whole-rock samples have NK/A >1, with 20 samples >1.5. The highest NK/A (1.68; sample 022) comes from a sample of indurated volcanic ash, and the peralkalinity may have been affected through heating of the ash layer by subsequent eruptions. The major-element data for the peralkaline rocks were assessed for posteruptive alkali loss (e.g., through hydration) using the molar FK/Al (FeO, K_2O, Al_2O_3) criteria of Macdonald (1974). All samples fell inside the 95% confidence lines and therefore are deemed not to have suffered any significant alkali loss.

[1]GSA Data Repository item 2012337, including a document detailing sampling and analytical techniques, supplementary figures, a map of sampling locations, BSEM images of representative textures, CL and BSEM images of zircons located in a comendite sample, argon-argon age spectrum of dated samples, and supplementary data tables, is available at http://www.geosociety.org/pubs/ft2012.htm or by request to editing@geosociety.org.

FIELD RELATIONSHIPS

The sampled units (see Table 1; see also supplementary Fig. 1 and supplementary Table 1 [see footnote 1]), together with NERC ARSF aerial photographs, were used to create a new geological map of Dabbahu (Fig. 3[2]), which illustrates the field relationships. Photographs of typical terrain are provided in Figure 4. An interpretation has been made of nonsampled units, based on surface morphology, which ideally requires confirmation through further field work. Demonstrably, the rock units were not emplaced in a strict order of increasing SiO_2 content as previously suggested (Barberi et al., 1974b). For example, trachytes have only been found stratigraphically beneath basaltic trachyandesite units, and early metaluminous rhyolites underlie intermediate units (Figs. 3 and 4). Field relationships of each of the principal rock units are summarized next.

Basalts

Sampled Dabbahu basalts are limited to two basalt flows, a dike, a gabbro lithic fragment, and a scoria cone called Dille (12°34′43″N, 40°23′34″E). Two of the basalt flows are exposed in ephemeral river beds: One is located in the extensive drainage system NW of the edifice where basalt is exposed beneath thin basaltic trachyandesite flows (e.g., Fig. 4E), and the other was emplaced below the trachyandesite flows to the SW of the edifice, close to Dille. The scoria cone itself is interbedded with a thin layer of pantellerite pumice. Pantellerite flows have only been located on the summit of Dabbahu, and it is likely that this pumice originated from the explosive counterpart of one of these eruptions. It is therefore proposed that the emplacement of the scoria cone was coeval with one or more of the pantellerite eruptions of Dabbahu. A complex of five basaltic dikes rises above the surrounding lava plain to the NW of the Dabbahu edifice. A coarse-grained lithic fragment is the only evidence of gabbroic-type rocks observed in the vicinity of Dabbahu and was found in a 10-m-deep canyon eroded through layers of explosive material (pumices, bombs, and lithics), between Ado Da'Ure and Aso Da'Ure (Fig. 4G). The main Dabbahu basalts are located to the south of the edifice summit, which is the northern extremity of the Manda-Hararo rift zone, where geologically recent flows can be seen to have erupted over older basalts. The erupted volume of Dabbahu basalts is difficult to estimate, particularly as the boundary

[2]Figure 3 is on a separate sheet accompanying this issue.

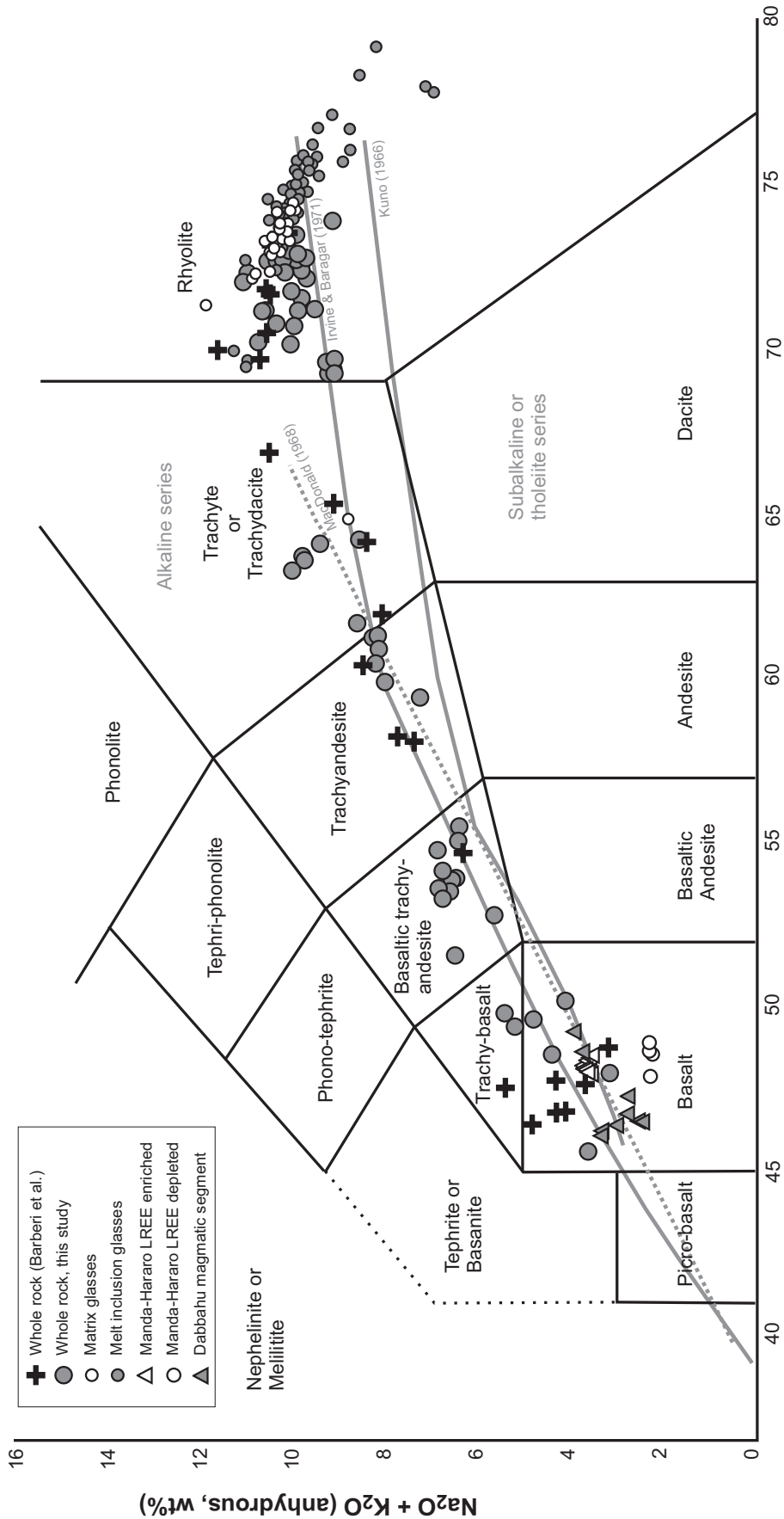

Figure 2. Total alkalis-silica diagram (Le Maitre, 2002). Dabbahu samples range from basalts through to peralkaline rhyolites (anhydrous normalized). Whole-rock samples (large gray circles) and matrix glasses (small white circles) are both from this study, melt inclusion glasses (small gray circles) are from Field et al. (2012b), black crosses indicate Dabbahu whole-rock analyses from Barberi et al. (1974b), gray triangles are Dabbahu magmatic segment whole-rock (2007 and 2009 eruptions) from Ferguson et al. (2010), and Manda-Hararo rift segment light rare earth element (LREE)–enriched (white triangles) and LREE-depleted samples (large white circles) are from Barrat et al. (2003). Gray lines represent the division between alkaline and tholeiite (subalkaline) series from Kuno (1960), MacDonald (1968), and Irvine and Baragar (1971).

TABLE 1. REPRESENTATIVE XRF MAJOR-ELEMENT ANALYSES

TAS definition:	Basalt	Basalt	Basalt	Trachy-basalt	BTA	BTA	Trachy-andesite	Trachy-andesite	Trachyte	Trachyte	Trachyte	Rhyolite	Rhyolite	Rhyolite	Rhyolite	Rhyolite	Rhyolite	Rhyolite	Rhyolite
Subdivision:*	T	T	T	H	M	M	B	B			C	C	C	M	M	P	P	P	P
Sample:	LFAF08 040	LFAF08 044	LFAF08 045	LFAF08 028	LFAF08 006	LFAF08 025	LFAF08 066	LFAF09 100	LFAF08 032a	LFAF08 048	LFAF08 011	LFAF08 029	LFAF08 054	LFAF08 026	LFAF09 112	LFAF08 007C	LFAF08 055	LFAF08 061	
SiO_2	49.54	47.45	48.69	49.40	54.61	54.87	59.86	58.73	63.43	64.41	70.06	70.00	70.49	68.84	68.47	72.49	72.75	73.26	
TiO_2	2.13	1.86	3.39	3.61	2.04	2.41	1.67	1.62	0.71	0.78	0.34	0.40	0.33	0.43	0.45	0.37	0.36	0.32	
Al_2O_3	16.70	14.94	14.95	13.45	15.97	13.81	14.54	13.95	14.30	15.27	13.75	12.10	13.55	13.83	13.67	9.40	9.32	10.11	
$Fe_2O_{3(T)}$	10.71	10.65	14.39	14.91	10.04	12.38	8.49	8.45	8.31	7.80	4.67	5.69	4.60	5.00	5.27	6.59	6.60	5.76	
MnO	0.17	0.18	0.23	0.27	0.22	0.31	0.23	0.24	0.32	0.21	0.15	0.18	0.14	0.14	0.15	0.21	0.21	0.18	
MgO	5.42	8.48	4.74	4.51	2.80	2.78	1.74	1.47	0.44	0.34	b.d.	b.d.	b.d.	b.d.	0.18	b.d.	b.d.	b.d.	
CaO	9.70	11.39	9.06	7.79	6.36	5.47	3.75	4.40	2.56	2.15	0.95	0.67	0.70	1.54	1.68	0.29	0.27	0.27	
Na_2O	2.98	2.50	3.44	3.89	4.27	4.89	5.06	4.96	5.68	5.59	5.75	6.20	5.59	4.89	4.81	6.08	5.99	5.77	
K_2O	1.03	0.58	0.96	1.29	2.09	1.97	3.08	2.90	2.79	4.30	4.25	4.48	4.33	4.27	4.18	4.37	4.25	4.27	
P_2O_5	0.26	0.21	0.41	0.82	0.65	1.17	0.48	0.80	0.13	0.15	0.02	0.02	0.01	0.04	0.06	0.01	0.01	0.01	
SO_3	0.01	0.56	0.02	0.09	0.04	0.06	0.08	0.55	0.04	0.02	0.02	0.07	0.01	b.d.	0.02	0.03	b.d.	b.d.	
LOI†	1.83	0.93	0.88	0.14	2.10	0.17	1.02	1.61	1.85	0.68	1.28	0.60	0.66	0.63	0.18	0.42	0.16	0.67	
Total	100.49	99.74	101.14	100.17	101.18	100.29	100.00	99.66	100.57	101.72	101.15	100.39	100.35	99.63	99.10	100.25	99.92	100.49	
NK/A§	0.36	0.32	0.45	0.58	0.58	0.74	0.80	0.81	0.87	0.91	1.02	1.24	1.02	0.92	0.91	1.57	1.55	1.40	

Note: TAS—total alkali versus silica diagram; BTA—basaltic trachyandesite; b.d.—below detection. X-ray fluorescence (XRF) analysis was carried out at Leicester University. Units in wt%.
*Abbreviations: T—transitional; H—hawaiite; M—mugearite; B—benmoreite; C—comendite; M—metaluminous; P—pantellerite.
†LOI—loss on ignition.
§NK/A—indication of peralkalinity.

between the Manda-Hararo basalts has not yet been clearly delimited. It is reasonable to propose that the basalts are the main component of the edifice, as evidenced by exposure in river beds, and therefore will comprise the bulk of the total estimated volume (>115 km^3).

Trachybasalts

A striking, low-lying (<5-m-high) SE-NW flow is visible from aerial photographs and satellite images (Fig. 3; supplementary Fig. 1 [see footnote 1]), just north of the Dabbahu edifice (~0.3 km^3). This is the only sampled trachybasalt flow. Its composition is sodic (defined as hawaiite). The source vent of this flow cannot be determined because it is now covered by Dabbahu rhyolites. At the base of the flow, there is a comenditic obsidian flow; magma mingling between the two rock types is visible on a macro- to a microscale.

Basaltic Trachyandesites

Basaltic trachyandesite lavas constitute one of the most extensive rock units at Dabbahu, with a conservative estimated volume of surface lavas of ~9 km^3. Sampled basaltic trachyandesites are located to the NW of Dabbahu and on the eastern side of the edifice itself. They underlie most of the other rock types except the basalts. The basaltic trachyandesite flows may have completely covered the edifice prior to eruption of the later peralkaline units. The eruption source for the basaltic trachyandesite lavas is not clear due to burial by later units; however, a small pit crater, ~0.75 km in diameter, is partially exposed east of the summit and has since been partially infilled with peralkaline products (Fig. 4F). The basaltic trachyandesite lavas form the rim of this caldera, suggesting this was one of the source vents. The scoria cones to the NW of Dabbahu have also erupted basaltic trachyandesite products. Potassic basaltic trachyandesite products (shoshonites) are found stratigraphically below the sodic basaltic trachyandesite products (mugearites).

Trachyandesites

Trachyandesites are located to the SW of Dabbahu, where they are seen to have flowed over and around a large metaluminous rhyolite flow. It is difficult to define the exact extent of this series of flows from aerial photographs due to the extensive pumice cover. All flows are sodic trachyandesite (benmoreite), except one sample, which is more potassic (latite). This was collected from the base of the flow front, and the age relationship is unclear with regard to the

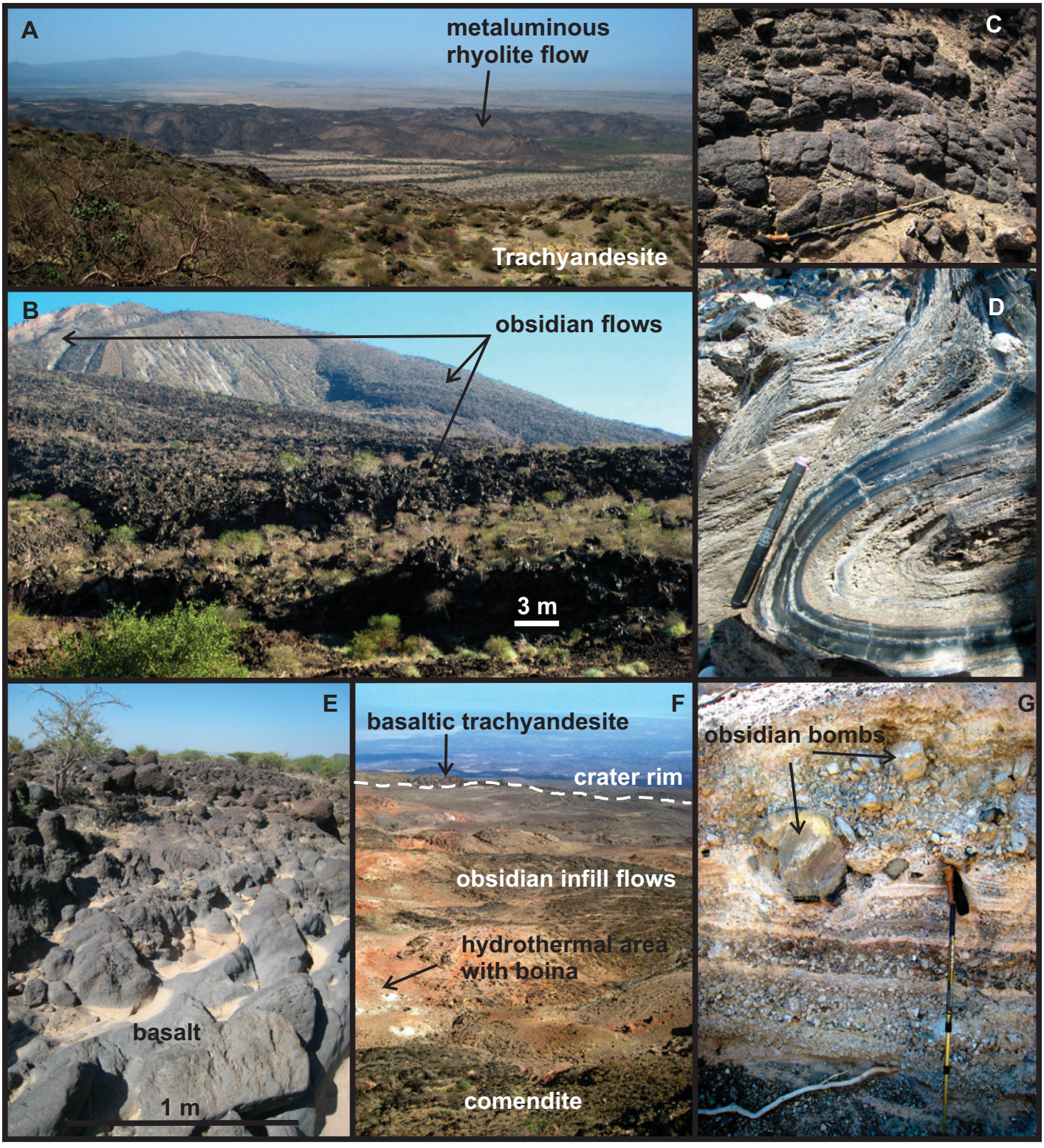

Figure 4. Field photographs of Dabbahu and its geology. (A) A view of the large metaluminous rhyolite flow to the SW of Dabbahu. Flow is up to ~100 m high. (B) Obsidian flows on the northern side of Dabbahu. (C) Polygonal surface of a trachyandesite (walking pole is ~1 m long). (D) Flow texture in an obsidian flow (pen for scale). (E) Basalt exposed in an ephemeral river bed, NW Dabbahu. (F) Small crater east of the summit partially infilled with obsidian flows. This crater is hydrothermally active and contains many boina (fumaroles used to condense water by the Afari pastoralists). (G) Layers of pumice, ash, lithic fragments, and obsidian bombs in an eroded canyon north of Aso Da'Ure (walking pole is ~1 m high).

other trachyandesite flows. Flows are typically hummocky, up to ~4 m high, with polygonal cooling joints (Fig. 4C). Their erupted volume is estimated at ~0.4 km^3.

Trachytes

Trachytes are limited in extent at Dabbahu, and the only surficial trachyte is a fractured and fragmented dome located to the SW of the Dabbahu edifice, just south of Dille (erupted volume ~0.15 km^3). The remaining two trachytes sampled are located in ephemeral stream beds beneath surface flows of basaltic trachyandesite.

Rhyolites

Metaluminous and peralkaline rhyolitic obsidians comprise a SW-NW band across Dabbahu (Fig. 3). On the edifice itself, rhyolites dominate the summit region and the northern section. Metaluminous rhyolites have been sampled in the north and southwest of Dabbahu. The prominent flow to the southwest is up to ~100 m high, with distinct semicircular flow ridges visible from the aerial photographs and a fingered flow front (Fig. 4A; supplementary Fig.1 [see footnote 1]). This flow was previously interpreted as intermediate composition by Barberi et al. (1974b); it shares similar morphological features to intermediate flows in the N and NW, in particular, the fingered nature of its flow front. A key difference is the substantial height of this flow (up to100 m above the surrounding plain). The rhyolite is one of the most physically weathered samples present at Dabbahu, and from field evidence, one of the oldest of the Dabbahu edifice. It underlies the trachyandesite flows that surround it and cover its source. To the north, there is another equally weathered flow, which is ~30 m high but has rounded flow fronts. This flow predates the overlying pantelleritic obsidian flows. A number of unsampled flows to the northeast, observed in aerial photographs, closely resemble both of the sampled flows, and these could also prove to be metaluminous. The volume of erupted metaluminous lavas is therefore difficult to assess, but it is at least 1.9 km^3. The remaining metaluminous sample is a dike located in an ephemeral river bed, overlain by sedimentary flood deposits, just north of the prominent SW flow. The dike has a bulk composition very similar to this major flow, and it is likely a coeval feature.

The domes to the north of Dabbahu (Alcoma, Gab'ho, the Da'Ure group) are all comenditic obsidians covered with various thicknesses of pumice. Comendites are also located on the summit, and one flow is found to the NNW of Dabbahu. However, only one comendite from Dabbahu itself is obsidian. Field evidence shows that these Dabbahu flows are older than the pantellerite flows, are more weathered, had a higher viscosity, and formed rounded flow fronts. It is likely that comendite flows are largely responsible for the topography underlying the pantellerites at the summit. The volume of peralkaline products is small; estimation of the visible erupted products is ~5.5 km.

The pantellerite flows cap the northern half of the Dabbahu edifice and are distinctive due to their sinuous nature (Fig. 4B; supplementary Fig.1B [see footnote 1]). The northern flows were erupted from a series of N-S fissure systems. Just to the south of this system, the summit pantellerites were erupted from a small pit crater (~0.15 km, 12°35′41.27N, 40°28′44.62E), which sits within an inferred larger caldera (~0.8 km × ~1 km). The obsidians flowed over this second caldera's rim. There are also small obsidian flows partially infilling a partially exposed pit crater (~0.75 km diameter) to the east of the summit (Fig. 4F). The flows to the east are heavily pumice-covered and thus predate those to the west. Flow banding is often observed within the obsidian flows (Fig. 4D).

Pumice

It has been suggested that pyroclastic products are scarce at central volcanoes in Afar (Lahitte et al., 2003b). However, pyroclastic material in the form of pumice is extensive at Dabbahu, with up to ~10 m of pumice covering underlying flows, and extensive pumice outwash rafts in the plains to the SW of Dabbahu. Trachytic pumice was found below comendite pumice to the north of Dabbahu. Comenditic pumice covers Ado Da'Ure, Aso Da'Ure, Gab'ho, and the area to the NE of Dabbahu (Fig. 3). A canyon has formed through drainage erosion between Ado Da'Ure and Aso Da'Ure, and ~10 m of pumice layers and obsidian bombs can be seen (Fig. 4G). Pantellerite pumice is found to the NE, covering the pantellerite obsidian flows in up to ~8 m of pumice. The basaltic trachyandesite and trachyandesite flows to the S and E are also covered in pantellerite pumices. The basaltic scoria cone of Dille contains a thin layer of pantellerite pumice. Immediately west of the Dabbahu summit, there lies an extensively pumice-covered slope that has been cut by deep erosion gullies.

Caldera and Fissure Systems

Several elliptical structures have been identified on and near the summit of Dabbahu (Fig. 3), and have been interpreted as pit craters or small caldera structures, although further field work would be required to confirm this hypothesis. One such inferred structure (12°35′46″N, 40°29′22″E) is a key area for "boina" (fumaroles adapted by the Afar pastoralists to condense drinking water). This relatively flat elliptical area is ringed by basaltic trachyandesite on the southern side and is concealed on the northern margins by thick comenditic flows. The elliptical area is partially infilled with rhyolites and hydrothermally altered material. A second elliptical vent area at the summit is surrounded by pantellerite obsidians. Fault systems and other structures are suggestive of four potential underlying caldera structures that may have been infilled by subsequent lava flows. The eccentricity of these structures is consistent with slight extension, probably related to rifting. The strike of the largest inferred caldera is ~340°, which is consistent with other faults on Dabbahu and in the rift axis immediately south of the edifice. The majority of pantellerites have been erupted from fissures, particularly two major fissure systems on the northern side of the edifice, which are orientated roughly N-S in line with the general direction of faulting on Dabbahu and elsewhere in this region (Fig. 3). The Dabbahu calderas or pit craters are substantially smaller than calderas developed on composite volcanoes to the south, in the northern Main Ethiopian Rift, which can be several kilometers across (e.g., Acocella et al., 2002).

^{40}Ar-^{39}Ar Geochronology

The only previously published dates for Dabbahu used fission-track or K-Ar dating methods, two of which were from the same sample (Barberi et al., 1974b). The exact locations of the dated samples have not been published. However, all are obsidian, which limits their localities to the summit and the northern half of Dabbahu, which are the youngest rocks. No radiogenic Ar was detected in three of Barberi et al.'s (1974b) samples, so a maximum age value was calculated assuming a radiogenic Ar content equal to 10% of the total ^{40}Ar. The range of dates obtained is 0.01 Ma (fission track) to 1.15 Ma (K/Ar, maximum age value). The authors themselves noted that the values obtained were extremely high, and it is the fission-track ages of 44 ka and 10.5 ka that are quoted as the preferred dates for obsidian emplacement at Dabbahu (e.g., Barberi et al., 1974b; Woolley, 2001).

Nine new ^{40}Ar-^{39}Ar dates were obtained for Dabbahu samples (Fig. 5; Table 2). The basaltic trachyandesites are the oldest samples dated, with a sample just north of the main edifice (sample 025) yielding a maximum age of 63.6 ± 3.5 ka (refer to supplementary Fig. 4 for age spectra [see footnote 1]). This sample

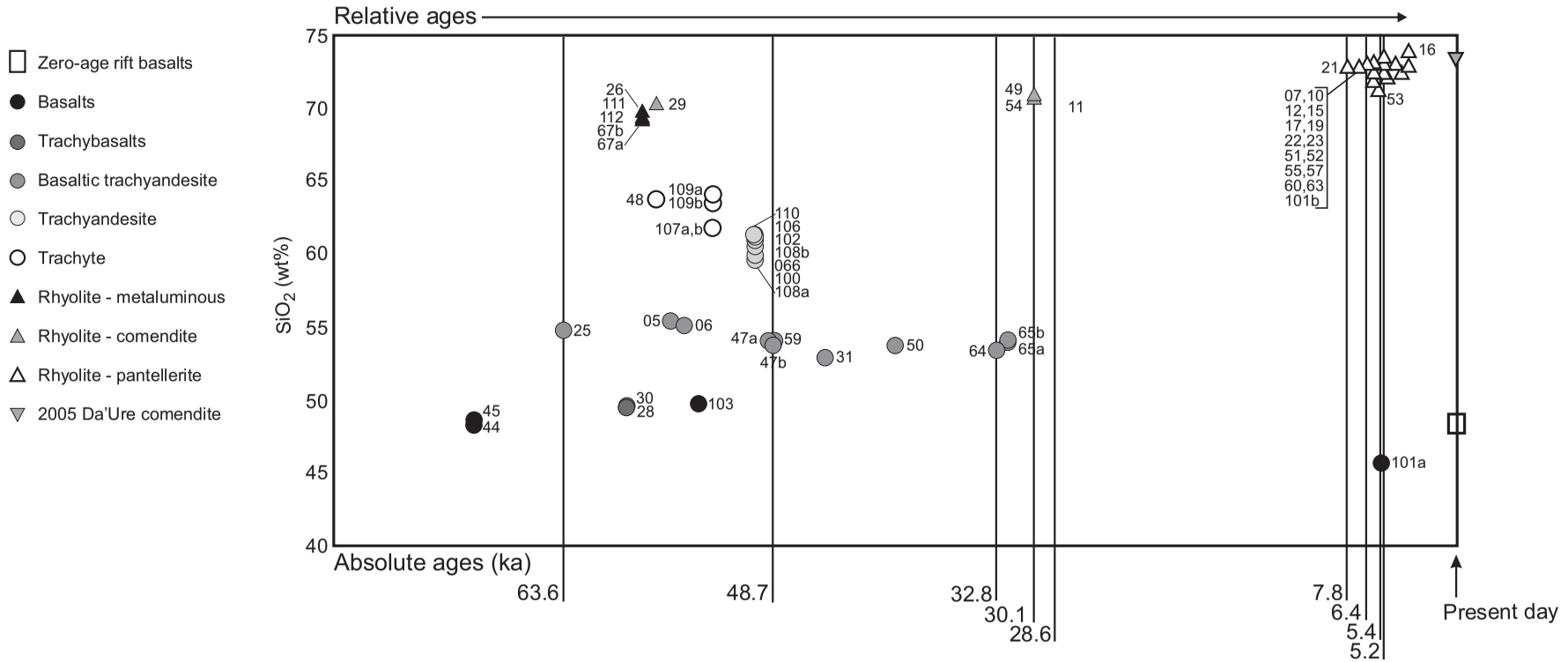

Figure 5. Estimate of relative ages vs. SiO_2 (wt%) content (anhydrous normalized basis), based on field relations for Dabbahu (excludes most pumices, and other centers, e.g., Gab'ho). Absolute ^{40}Ar-^{39}Ar ages (ka) are indicated by vertical lines that pass through dated samples. Zero-age rift basalts are from Ferguson et al. (2010). Sample numbers are indicated adjacent to symbols.

TABLE 2. ^{40}Ar-^{39}Ar GEOCHRONOLOGY

Sample	Rock type*	Method†	Plateau % ^{39}Ar [steps, °C]	Age (ka)§	Isochron age %^{39}Ar [steps, °C]	MSWD#	Isochron age (ka)	% ^{39}Ar [steps, °C]	MSWD	$^{40}Ar/^{36}Ar_i$	Total gas age (ka)
LFAF08 025	BTA	Separate	31 [1075–1100]	63.6 ± 3.5	31 [1075–1100]	0.03	33.5 ± 8.8	80 [900–1300]	3.02	309.0 ± 5.3	138.0 ± 2.6
LFAF08 047	BTA	Grndms	63 [550–850]	48.7 ± 5.9	63 [550–850]	0.63	30.1 ± 19.2	63 [550–850]	0.7	300.8 ± 12.4	43.6 ± 4.7
LFAF08 064	BTA	Grndms	67 [550–850]	32.8 ± 3.2	67 [550–850]	0.44	31.5 ± 9.8	67 [550–850]	0.65	295.8 ± 5.0	20.0 ± 2.7
LFAF08 054	Comendite	Grndms	60 [550–750]	30.1 ± 0.4	60 [550–750]	1.34	29.148 ± 3.194	60 [550–750]	1.94	299.4 ± 31.5	29.7 ± 0.4
LFAF08 011	Comendite	Grndms	81 [550–850]	28.6 ± 0.7	81 [550–850]	0.57	27.845 ± 2.352	81 [550–850]	0.81	296.5 ± 7.0	24.9 ± 0.7
LFAF08 021	Pantellerite	Separate	94 [850–1500]	7.8 ± 4.3	94 [850–1500]	5.79	25.2 ± 11.2	94 [850–1500]	5.76	289.1 ± 8.3	11.1 ± 1.7
LFAF08 019	Pantellerite	Separate	96 [850–1400]	6.4 ± 2.7	96 [850–1400]	2.56	14.2 ± 13.9	96 [850–1400]	3.69	292.7 ± 10.9	8.0 ± 1.5
LFAF08 055	Pantellerite	Separate	99 [800–1500]	5.4 ± 1.8	99 [800–1500]	3.77	11.8 ± 4.4	99 [800–1500]	3.28	289.3 ± 8.6	5.0 ± 0.9
LFAF08 063	Pantellerite	Separate	89 [875–1400]	5.2 ± 3.4	89 [875–1400]	4.62	42.0 ± 21.3	89 [875–1400]	4.9	280.9 ± 19.2	5.9 ± 1.3

*As determined by X-ray fluorescence (XRF). BTA—basaltic trachyandesite; comendite and pantellerites are obsidians.
†Method—analysis of groundmass (Grndms) or anorthoclase separates.
§Preferred age.
#MSWD—mean square of weighted deviates.

yielded a U-shaped spectrum, suggesting either: (1) a mixed population of crystals or (2) excess argon, and therefore the weighted mean of the youngest steps is favored as a maximum age. This sample overlies the original basalts from Dabbahu (Fig. 3), indicating that Dabbahu began to evolve prior to ca. 67 ka. The peralkaline rhyolites were dated by anorthoclase separates, which potentially provide an age slightly older than that of eruption (Esser et al., 2004). The oldest dated comendite rhyolite (30.1 ± 0.4 ka), which overlies basaltic trachyandesite lavas to the E of the summit, overlaps within error of the youngest dated basaltic trachyandesite (32.8 ± 3.2 ka), suggesting that the comenditic eruptions may have commenced close to the waning of basaltic trachyandesite eruptions, or soon after they had ceased. This is supported by the field evidence, as the peralkaline rhyolites overlie all other rock units. The pantellerite obsidians are all younger than 7.8 ± 4.3 ka (sample 21, stratigraphically the oldest sampled pantellerite, located at the base of an eroded canyon on Myramcoma just north of the summit of Dabbahu). The western obsidians that are not pumice-covered were erupted after the pumice-covered Molicoma obsidians to the east of the summit. However, the age errors on both these sample types overlap, and relative ages rely on field evidence (Fig. 5). These anorthoclase-bearing samples are young and were problematic to date. A step-heating fractionation effect can result in early gas containing excess ^{36}Ar and ^{39}Ar, making the age young, whereas late gas fractions can be enriched in residual ^{40}Ar, yielding old apparent ages.

The dates obtained as part of this study are significantly younger than those obtained by Barberi et al. (1972). Taking into consideration the new dates, field relationships, and stratigraphy, Dabbahu must have begun to erupt some, relatively short, time prior to the oldest date obtained by us (i.e., >67 ka) and has remained active to the present day (Fig. 5).

Petrography

The Dabbahu samples are weakly to highly porphyritic (0–47 vol% phenocrysts), with an average phenocryst content of 7% overall (median 4%: Fig. 6). The basalts are the most porphyritic samples, with plagioclase dominating a phenocryst assemblage of plagioclase + clinopyroxene (diopside and augite) + olivine ± magnetite ± apatite, set in holocrystalline groundmass containing the same minerals. One basalt sample has distinct euhedral olivines (~2 mm) with prominent Fe-rich rims (supplementary Fig. 2A [see footnote 1]). The gabbroic sample displays alteration textures, particularly in olivine crystals, which show extensive alteration to iddingsite.

The trachybasalt samples have a low percentage of phenocrysts (2–5 vol%). Their phenocryst assemblage is alkali feldspar + plagioclase + augite + olivine + magnetite. The feldspars range from bytownite through to minor anorthoclase; the anorthoclase is an indication of some minor magma mixing in these samples. Phenocrysts are up to 2 mm in size. Both samples have a crystalline groundmass and show signs of disequilibrium with embayed and rimmed phenocrysts, e.g., ribbon corona, ~60 µm wide, surrounding the plagioclase (supplementary Fig. 2B [see footnote 1]). Glassy blebs are visible in the matrix in thin section.

Textures vary among the basaltic trachyandesite samples; some are consistently vesicular, while others are hypocrystalline with low vesicularity. They are weakly to highly porphyritic (0.8%–17% phenocrysts by volume) within a fine-grained groundmass. The assemblage is plagioclase + olivine + magnetite ± clinopyroxene ± ilmenite ± apatite ± rare alkali feldspar, with minor $FeS_{(1-x)}$ found in the groundmass of two samples. Clinopyroxenes have a range of compositions dominated by augites with minor ferro-hedenbergites, while feldspars range from bytownite to anorthoclase. Higher proportions of basaltic trachyandesites contain ilmenite than any other rock type. These ilmenites largely occur in glomerocrysts, which are up to ~4 mm across, and contain numerous inclusions of apatite and Fe-Ti oxides. Skeletal crystals of olivine and Fe-Ti oxides abound (supplementary Fig. 2C [see footnote 1]). Several basaltic trachyandesites have noticeably distinctive groundmass textures, i.e., separate patches of coarse- and fine-grained groundmass with a sharp divide between.

Trachyandesite samples have 6–22 vol% phenocrysts and an assemblage of plagioclase + augite + olivine + magnetite ± ilmenite ± apatite ± rare alkali feldspar. Feldspars range from bytownite to minor anorthoclase. $FeS_{(1-x)}$ is found in the groundmass of most trachyandesites. Plagioclase phenocrysts (~1 mm length) have distinct sodic rims over more calcic cores.

The trachyte lavas are similar to trachyandesites with regard to phenocryst content (6%–18%) of plagioclase + augite + olivine + magnetite ± apatite ± alkali feldspar ± rare ilmenite; however, the trachyte pumice has <1% phenocrysts, comprising just plagioclase. Clinopyroxene is often radially intergrown with plagioclase. The feldspars range from labradorite through to anorthoclase. Cristobalite crystals (~400 µm) were found in one sample (supplementary Fig. 2D [see footnote 1]). The groundmass is glassy, often with quench textures. All trachytes have disequilibrium textures in the phenocrysts, such as resorbed clinopyroxene overgrown by thin Fe-rich rims (supplementary Fig. 2E [see footnote 1]). Magnetite occasionally shows exsolution textures suggestive of slow cooling.

The metaluminous rhyolites have consistent phenocryst contents (5%–8%) of clinopyroxene + olivine + magnetite + apatite ± alkali feldspar ± ilmenite set in glassy groundmass dominated by feldspar microlites. Feldspar compositions range from andesine through to anorthoclase, and the bulk of clinopyroxenes are augites with minor ferro-hedenbergite. Rare euhedral zircons (~20 µm) were located in one sample. Apatite is abundant, in some cases forming clusters around phenocryst rims. Many of the oxides show exsolution textures indicative of slow cooling. Olivines have undergone some alteration to Fe-rich iddingsite. Plagioclase phenocrysts are often euhedral, but other phenocrysts are rounded and embayed.

Comendites are texturally highly variable; some are aphyric, whereas porphyritic examples contain up to 12% phenocrysts, which are dominated by alkali feldspar ± clinopyroxene ± olivine ± apatite ± ilmenite ± magnetite, in a glass matrix. The majority of feldspars are anorthoclase, with plagioclase found in only one sample (029), and these are small crystals (200 µm) located within trachybasalt blebs. Clinopyroxene is largely augite to ferro-hedenbergite in composition: One sample contains rare grains of another clinopyroxene of aegirine-augite composition. $FeS_{(1-x)}$ is found as groundmass or inclusions in two thirds of samples. An obsidian from Gab'ho contains numerous euhedral zircons <40 µm in diameter (supplementary Figs. 2G and 3 [see footnote 1]). Some comendites show signs of magma mingling, visible on all scales.

Pantellerites have an average phenocryst content of <2%, with a range of 1%–11% in the porphyritic samples. Pumices are generally aphyric, with minor microlites or very rare phenocrysts. The pantellerites are dominated by anorthoclase with rare Na-sanidine and subordinate clinopyroxene (dominantly ferro-hedenbergite through to augite, with rare aegirine-augite) and minor apatite ± ilmenite ± fayalite ± aenigmatite (a sodium-iron-titanium inosilicate commonly identified in peralkaline lavas; Kunzmann, 1999). The most porphyritic pantellerite contains euhedral quartz (~600 µm), and quartz-feldspar granophyric textured intergrowths that may be xenocrystic in origin (<1 mm). Three other samples contain secondary cristobalite, and three samples contain $FeS_{(1-x)}$. A single amphibole crystal (~400 µm) was found (supplementary Fig. 2G [see footnote 1]). The pantellerites are all glassy and often very vesicular. Flow banding is common, caused by high concentrations

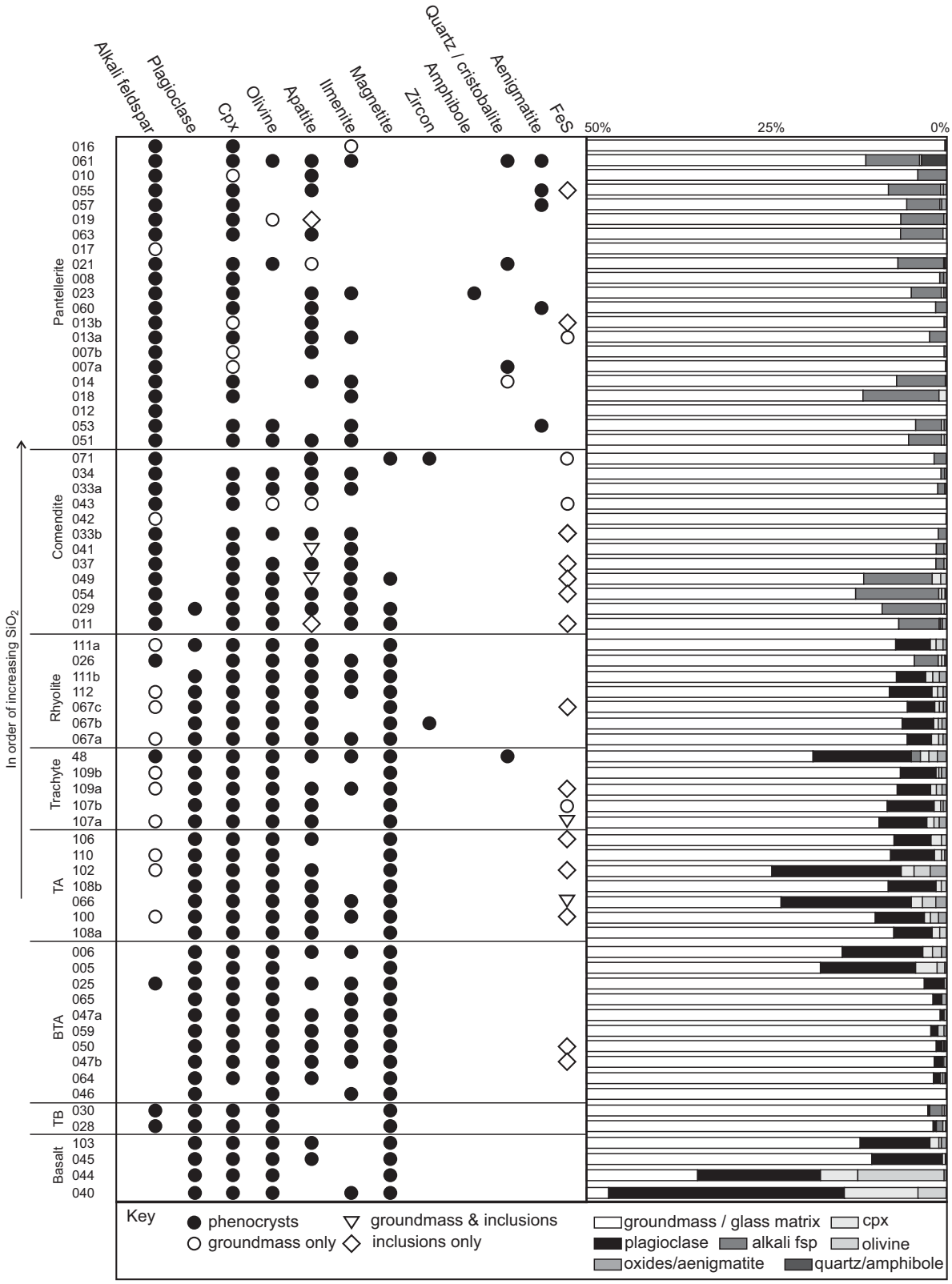

Figure 6. Summary of modal mineralogy of Dabbahu. Plot to left shows phenocryst assemblages (aphyric samples and some pumices omitted). Also indicated are minerals that occur as inclusions in other minerals or as groundmass. Bar chart to right shows percent volume of phenocrysts present in each sample. Each Dabbahu sample is composed of >50% groundmass or matrix glass, and this upper 50% matrix glass is not shown (i.e., horizontal scale is 0%–50%). Average phenocryst content of porphyritic samples <7 modal %. TB—trachybasalt, BTA—basaltic trachyandesite, TA—trachyandesite.

of microlites and/or vesicles. Alkali feldspar and clinopyroxene crystals are generally euhedral, although some show rounding suggestive of reheating and resorption. Aenigmatites are found as phenocrysts (up to 400 µm) in five samples (supplementary Fig. 2H [see footnote 1]) and comprise up to 10% of the total phenocryst content.

GEOCHEMISTRY

Major Elements

Representative major-element whole rock analyses are given in Table 1 (refer also to supplementary Table 2 [see footnote 1]) and plotted as Harker diagrams in Figure 7. New data are augmented by published analyses of Barberi et al. (1974b) from Dabbahu, and of Ferguson et al. (2010) and Barrat et al. (2003) for basalts from the Manda-Hararo rift segment. Some elements show smoothly curved variation in concentration with SiO_2, e.g., CaO (Fig. 7D) and MgO (Fig. 7B), due to changing composition or proportions of the major phenocryst phases. Others show kinks on Harker diagrams, e.g., Al_2O_3 or Na_2O, due to abrupt changes in the extracted phenocryst assemblage. In the case of , here is minor scatter beneath the peak, suggesting the possibility of some mixing (Marshall and Sparks, 1984) in basaltic trachyandesite samples. Al_2O_3, TiO_2, and Fe_2O_3 trends show a marked bifurcation at ~70 wt% SiO_2 (Figs. 7A, 7C, and 7E) into Fe- and Ti-rich, Al-poor pantellerites and Fe- and Ti-poor, Al-rich comendites. Fe enrichment and Al depletion are characteristic of pantellerite rocks (Noble, 1968). Melt inclusion glasses overlap with matrix glasses but extend the range in SiO_2 to higher values; melt inclusion glasses extend the trends to SiO_2 contents of almost 80 wt% (anhydrous).

The basaltic end of the Dabbahu whole-rock trend is defined by four analyses from this study and a further seven from Barberi et al. (1974b). They range from 4 to 10 wt% MgO, with Mg# (molar Mg/[Mg + Fe_t]) up to 47, and variable, but high, TiO_2, from 2 to 4 wt%. This compositional range is embraced by the light rare earth element (LREE)–enriched basalts of the Manda-Hararo rift (Barrat et al., 2003).

MINERALOGY

Low phenocryst content is a characteristic of the Dabbahu whole-rock samples (many pumices and peralkaline rhyolites are completely aphyric), suggesting a close approximation to liquid compositions. The mineralogy of the phenocryst-bearing samples is summarized in Figure 6. Feldspars are the dominant mineral phase, with plagioclase present at the mafic end, and alkali feldspar in the rhyolites. Plagioclase and alkali feldspar coexist in intermediate rocks. The mafic minerals clinopyroxene and olivine are present almost across the entire composition range from basalt to rhyolite; orthopyroxene is completely lacking. Ilmenite and magnetite coexist mainly in intermediate rocks, with more-evolved samples characterized by ilmenite alone. Quartz is found as a phenocryst in just one rhyolite (sample 061). Hydrous minerals are conspicuously lacking at Dabbahu; just one amphibole xenocryst was found in all samples studied.

In order to view the evolving mineral chemistry across such a wide range of rock types, we show mineral compositions for olivine, clinopyroxene, alkali feldspar, and plagioclase in Figure 8, with samples arranged in order of increasing SiO_2 along the vertical axis. We distinguish texturally between phenocryst cores and rims, and microlites or groundmass crystals. To facilitate comparison between the different mineral plots, we have left blank lines for samples that either lack a given mineral phase or for which mineral analyses were not obtained.

Feldspar

Feldspar occurs in almost every sample, either as a phenocryst, or in the groundmass (Figs. 6 and 8). It is the most common mineral, comprising up to 100% of the total phenocrysts in any one sample. Analyses are given in supplementary Tables 3 and 4 (see footnote 1). The Dabbahu feldspars cover a considerable range of compositions, from bytownite to sanidine, defining a smooth continuous variation across the feldspar ternary diagram (Fig. 8).

Plagioclase compositions range from bytownite to oligoclase. Plagioclase in the groundmass generally has a lower anorthite (An) content than the phenocrysts. Overall, there is a general decrease in An content with increasing SiO_2. This trend is most pronounced if one looks at the most An-poor plagioclase in each sample, which decreases from ~An_{50} in the basalts to An_{20} in the rhyolites. Plagioclase crystals are generally unzoned, but some show abrupt boundaries between adjacent zones suggestive of a sudden change in crystallization environment. Both normal and reverse zoning occurs. For most samples, the overall range in An content is <15 mol%, although several samples of trachyandesite and basaltic trachyandesite have plagioclase populations with very wide ranges in An. The greatest total range of feldspars is observed in trachybasalts, e.g., sample 028 has alkali feldspar cores ($An_{0.5}Ab_{69}Or_{30}$), plagioclase cores ($An_{78}Ab_{22}Or_0$), and plagioclase groundmass with intermediate compositions, suggestive of magma mixing. Petrographically, this sample shows mixing on all scales with a comendite (sample 029), and the thin section contains glassy blebs with a fine-grained quenched matrix, in contrast to the coarser groundmass of the main matrix.

Alkali feldspar composition is more restricted, particularly in the rhyolites. From the onset of alkali feldspar appearance as a major phenocryst phase, the Or content increases from 10 to 32 mol%. The average composition through the entire range of rhyolites is around $Or_{30}Ab_{68}$ (anorthoclase). The composition in the pantellerites is extremely restricted, with major anorthoclase, and minor sodic-sanidine. This is consistent with the view of Thompson and Mackenzie (1967), who suggested that pantellerites lie within a "low-temperature zone" that has its origin in the "thermal valley" of the granite system.

Minor elements vary little throughout the feldspars with very low values; MgO and FeO_t tend to be below detection in alkali feldspars; in plagioclase, MgO is generally below 0.2 wt%, while FeO_t varies up to 1 wt%.

Olivine

Olivine analyses are given in supplementary Table 5 (see footnote 1). Olivine occurs in all rock types, from basalt to rhyolite, as phenocrysts or groundmass. From basalts to comendite, the composition (calculated on a ternary basis) shows a decrease in forsterite (Fo) from Fo_{83} to nearly pure end-member fayalite (Fa_{96}), with MgO contents below detection. A plot of Fo content against sample number ranked in order of SiO_2 content (Fig. 8) shows a marked drop in Fo of ~20 mol% content between trachytes and rhyolites. A wide range of olivine compositions can be found within some individual samples of basalt and basaltic trachyandesite. Basalt sample 044, for example, contains euhedral olivines of composition $Fo_{83–76}$, with distinctive rims of $Fo_{80–57}$ (supplementary Fig. 2A [see footnote 1]). Where olivines are rimmed, the rim composition is either a lower Fo content than the cores, as for sample 044, or the rim compositions are bracketed by the range of core compositions. This behavior is suggestive of magma mixing between more- and less-evolved end members, producing hybrids with intermediate Fo contents.

The tephroite (Tp) component (Mn_2SiO_4) in the olivines increases systematically with decreasing Fo, and in rhyolites it can be significant (average Tp_5); the highest Tp component (Tp_{14}) is found in a comendite. These Dabbahu Tp values are higher than olivines from other pera-kaline systems, such as Olkaria (Kenya), which have $Tp_{\sim 0.3}$ (Marshall et al., 2009), and Pantelleria, which have up to Tp_7 (White et al., 2009).

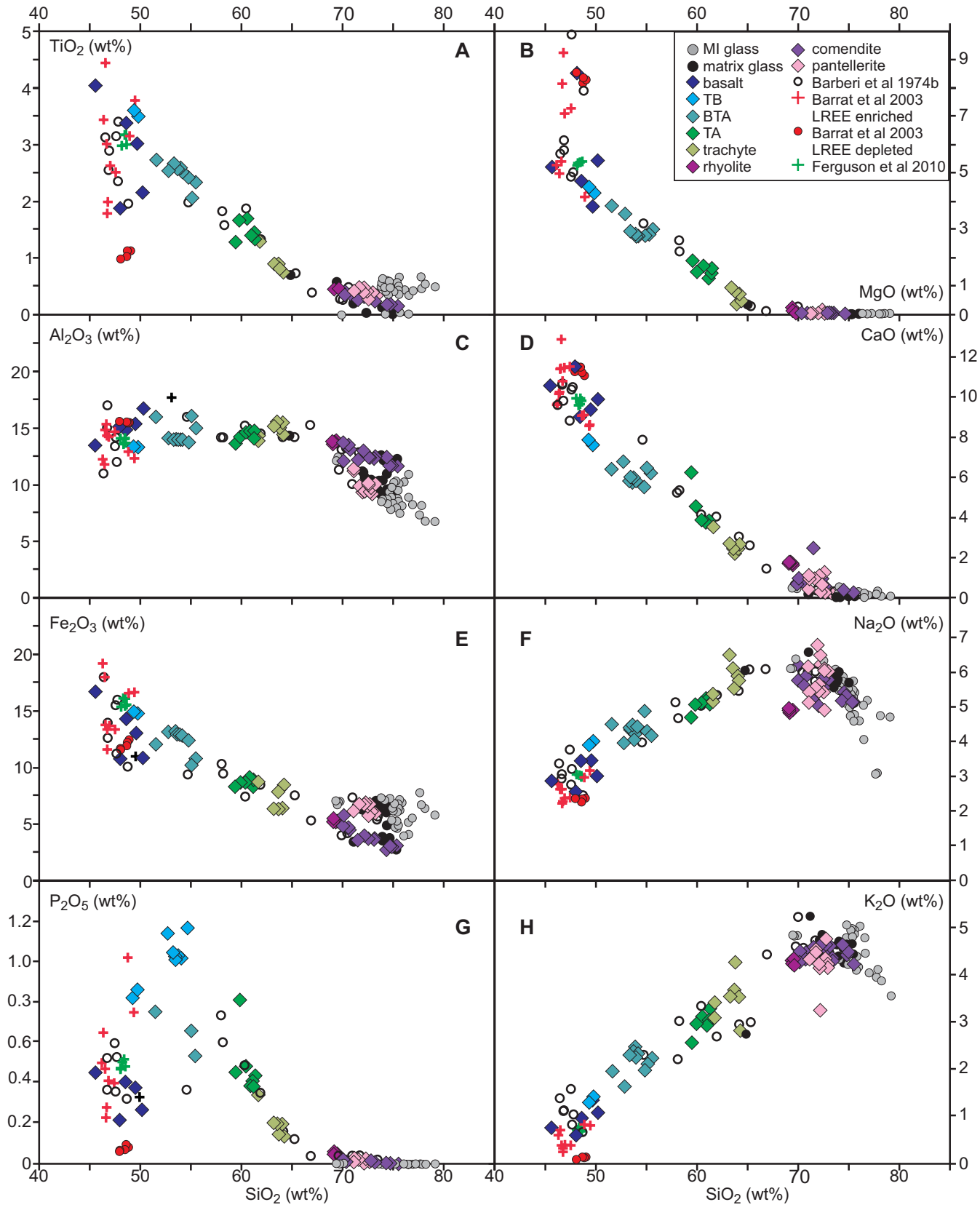

Figure 7. Selected major element vs. SiO_2 Harker diagrams for Dabbahu, together with samples from Barberi et al. (1974b), Manda-Hararo basalts from Barrat et al. (2003), and 2007 and 2009 rift basalts from Ferguson et al. (2010). Total Fe is plotted as Fe_2O_3*. TB—trachybasalt, BTA—basaltic trachyandesite, TA—trachyandesite.

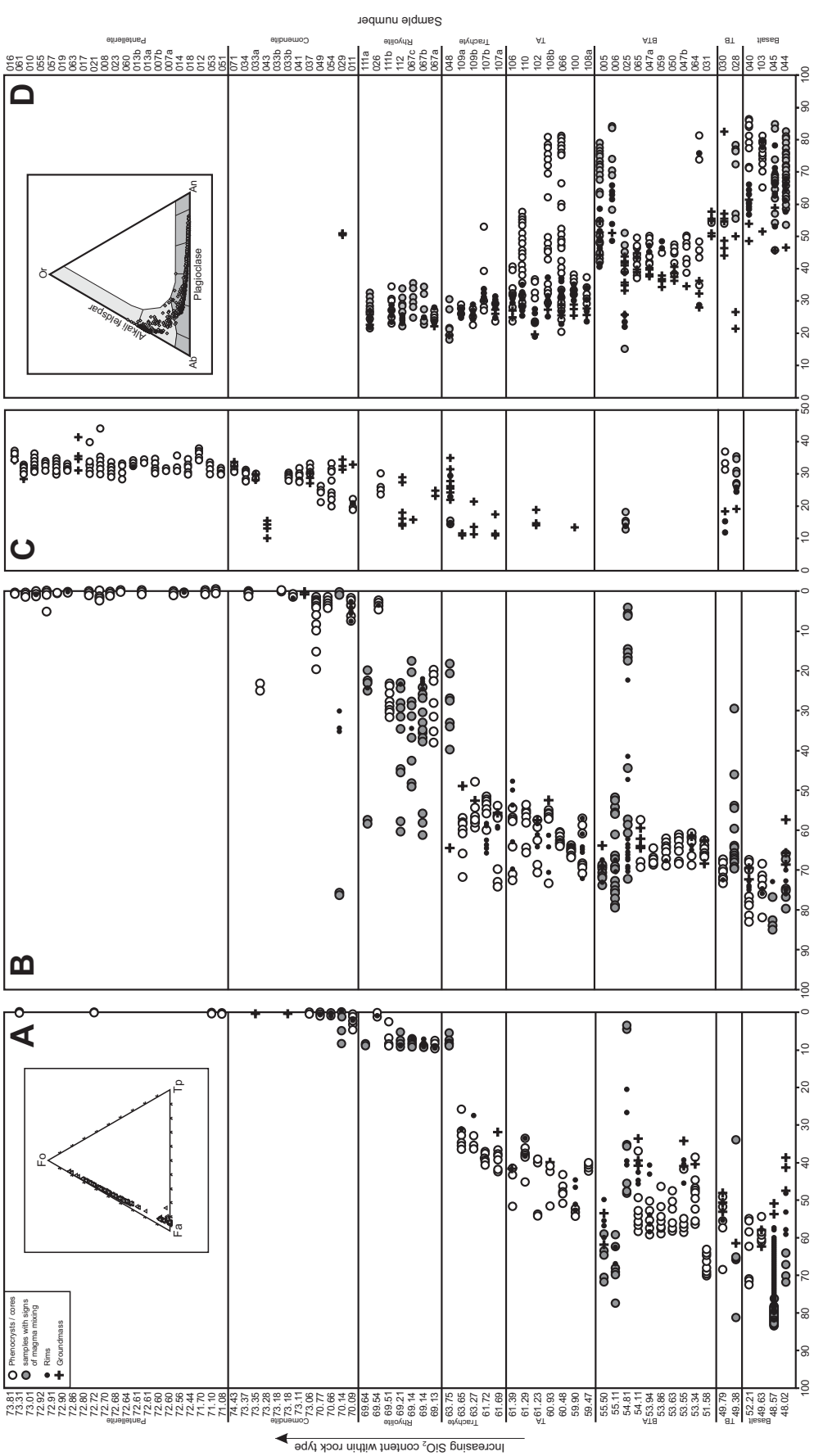

Figure 8. Mineral chemistry from Dabbahu samples arranged in order of increasing SiO_2 from bottom to top and categorized according to rock type (total alkalis-silica classification) for (A) olivine, (B) clinopyroxene (cpx), (C) alkali feldspar, and (D) plagioclase. Insets in A and D show the same data plotted into, respectively, the olivine (forsterite-fayalite-tephroite) and feldspar (orthoclase-albite-anorthite) ternary diagrams. Sample numbers are given up the right-hand axis; their SiO_2 contents (anhydrous) are given up the left-hand axis. Gray circles indicate samples that show signs of magma mixing, either at macro- or microscale. Blank lines denote either that that mineral was not present in that sample, or there is no analysis of that phase. TB—trachybasalt, BTA—basaltic trachyandesite, TA—trachyandesite.

Inclusions are found within the olivines, particularly apatite and Fe-Ti oxides and quenched melt inclusions, which are common in the basaltic trachyandesite, trachyandesite, and trachyte samples. In the rhyolites, metaluminous and comendite samples contain greater numbers of apatite and oxide inclusions in larger olivine crystals (<1.5 mm) than their pantellerite counterparts (<200 µm).

Clinopyroxene

Clinopyroxenes (cpx) are found within all rock types and range compositionally from Mg-rich augites and diopsides to Fe-rich augites (Fig. 8; supplementary Table 6 [see footnote 1]). Five aegerine-augites (Na-rich clinopyroxene) were identified from three peralkaline samples, in each case coexisting with augites. Clinopyroxene compositions show a steady decrease in Mg# from 85 in basalts through to zero in the comendites (Fig. 8). The 249 clinopyroxene analyses from pantellerite rhyolite samples show very limited differences in composition (Mg# of 0–5). The majority of basaltic trachyandesite, trachyandesite, and trachyte samples also show a generally restricted composition ~Mg# of 75–50. However, some samples show a large range of compositions, such as basaltic trachyandesite sample 025, which almost spans the entire range shown by all Dabbahu samples (Mg# 4–72), and the metaluminous rhyolite clinopyroxenes, which range from Mg# 3 to 62. This is suggestive of a component of magma mixing in these samples, but in some cases, it may be a result of incorporation of xenocrysts, or retention of a fraction of crystals from each increment of crystallization, i.e., imperfect crystal fractionation.

Clinopyroxene phenocrysts are diverse in appearance; they can occasionally be zoned, and appear as euhedral crystals, as radial intergrowths with plagioclase, as glomerocrysts, or as sponge-textured crystals that have been partially reabsorbed and then overgrown with distinct Fe-rich rims (supplementary Fig. 2E [see footnote 1]). The change in Mg# in the latter case is from 72 in the core to 50 in the rims. Two distinct populations of clinopyroxene cores are found in comendite sample 029—those which are close to diopside composition, and those which are ferro-hedenbergite. The rims around the ferro-hedenbergite crystals sit between the two core populations in composition, indicating this sample has been subjected to magma mixing prior to eruption.

Minor elements show some variation overall, e.g., MnO varies from 4 wt% in one trachyandesite crystal down to zero in the peralkaline crystals. However, the majority contain <1.6 wt% MnO. TiO_2 and Al_2O_3 contents decrease from basalt to the peralkaline rhyolites, ~4 to 0 wt% and 6 to 0 wt%, respectively. Na_2O shows an increase in range within each sample with increasing SiO_2; the maximum Na_2O is found in an aegirine-augite with 6 wt%. The higher values are limited to the peralkaline rocks; the bulk of the crystals contain <1 wt% Na_2O.

The FeO_t content ranges from 5 to 34 wt%. Calculated Fe^{3+} content, estimated from stoichiometry using the method of Schumacher (1991), shows that up to 43% of the FeO_t is Fe^{3+}, with the exception of one crystal that has a high proportion of 71%.

Fe-Ti Oxides

Ilmenite and titanomagnetite are found in all rock types except the trachybasalts, which contain magnetite only, and the pantellerites, which only contain ilmenite (Fig. 6). Coexisting pairs are rare. Analyses are given in supplementary Tables 7 and 8 (see footnote 1). The ulvöspinel component in the cores of titanomagnetite phenocrysts ranges from 21 to 82 mol% calculated using ILMAT (Lepage, 2003), with the Fe^{2+} and Fe^{3+} recalculation method of Carmichael (1967). The ilmenite component in ilmenite phenocrysts ranges from 50 to 99 mol%. All but two crystals are within the range 80–99 mol% (median 96 mol%). With regard to peralkalinity, magnetite is only found in the comendites (NK/A = 1.02–1.24), whereas ilmenite is found in both comendites and pantellerites (pantellerites NK/A = 1.32–1.55). This in part accounts for the trend of comendites to lower bulk FeO contents than pantellerites, which in turn may be indicative of slightly more reducing conditions in the pantellerites (e.g., Toplis and Carroll, 1995; White et al., 2005).

Aenigmatite

In alkaline lavas, aenigmatite ($Na_2Fe^{2+}_5TiSi_6O_{20}$) commonly occurs as a groundmass constituent and more rarely as phenocrysts, e.g., Fantale volcano, Ethiopia (Gibson, 1970). At Dabbahu, aenigmatites are found as phenocrysts up to 400 µm in length in five peralkaline rhyolite samples (supplementary Fig. 2H [see footnote 1]) in which the NK/A ranges from 1.32 to 1.55. The aenigmatites have a restricted compositional range, FeO = 41–43 wt%, TiO_2 = 8.2–9.5 wt% (supplementary Table 9 [see footnote 1]), and cluster at the aenigmatite end of the aenigmatite-wilkinsonite solid solution (Grew et al., 2008). Experimental studies on samples from Pantelleria were able to stabilize aenigmatite at temperatures below 900 °C (dry) and low oxygen fugacity (at or below fayalite-magnetite-quartz [FMQ]) (Kunzmann, 1999; White et al., 2005). Scaillet and Macdonald (2001) crystallized aenigmatite only at pressures <100 MPa. In contrast, recent experiments by Di Carlo et al. (2010) found that aenigmatite stability in pantellerites from Pantelleria required >2.8 wt% H_2O_{melt}, NK/A >1.2, and pressures >100 MPa.

Minor Phases

A single amphibole crystal (300 µm in length) was identified in pantellerite sample 023 (supplementary Fig. 2G [see footnote 1]). The amphibole (supplementary Table 10 [see footnote 1]) is a sodic amphibole (arfvedsonite), which is commonly associated with alkali granites. Textural evidence suggests the amphibole is xenocrystic. Very little experimental work has been carried out on the stability of arfvedsonite, but Ernst (1962) suggested arfvedsonite is stable in temperatures up to 712 °C at 200 MPa fluid pressure and low oxygen fugacity (iron-wüstite buffer). Plausibly, the amphibole was entrained from plutonic equivalents of the pantellerites.

Apatite is a common constituent of the more silica-rich rocks, and the majority of crystals are equant, with the occasional more elongate form. They are generally small (<20 µm), although they sometimes reach 100 µm in length. Zoning is discernible in many crystals, although too fine in scale to characterize chemically. Apatite is absent from all basalts and trachybasalts, except a single sample (103), where apatite inclusions are found in clinopyroxene. Apatite appears with more frequency in the basaltic trachyandesites through to rhyolites. It is found as discrete microphenocrysts, but more frequently as inclusions in olivines, clinopyroxene, Fe-Ti oxides, and plagioclase, particularly within the trachytes and metaluminous rhyolites where the phenocrysts contain a very high number of inclusions. This textural evidence suggests early saturation of apatite in these rocks, consistent with the observed peak in P_2O_5 content of whole rocks at ~55 wt% SiO_2 (Fig. 7G).

Zircons were found in only two samples: rare zircons in a metaluminous rhyolite (sample 067b), and numerous zircons in a mildly peralkaline comendite (NK/A = 1.09) from Gab'ho (sample 071). The zircons occur as euhedral microphenocrysts <40 µm in length (supplementary Fig. 2F [see footnote 1]). Cathodoluminescence analysis reveals concentric zoning and distinct cores with variable-width rims (see supplementary Fig. 3). Zircons occur most frequently in clusters, and are occasionally associated with alkali feldspar as single micro-

phenocrysts. The scarcity of zircon reflects the high solubility of this mineral in alkaline melts (Watson, 1979).

Quartz appears as a phenocryst in only one Dabbahu sample, a peralkaline rhyolite (061), where it is a relatively abundant component (2.9 modal %), forming euhedral crystals up to 500 µm in length. This tiny obsidian flow (~100 m × 3 m) is the most crystal-rich of the obsidians, with 11 modal % phenocrysts. This sample also contains quartz-feldspar overgrowth rims and granophyric intergrowths around feldspars, and quartz-feldspar spherules, potentially derived from silicic intrusive rocks and entrained within the ascending magma. Some pantellerites contain rare, anhedral crystals of cristobalite (supplementary Fig. 2D [see footnote 1]), generally <100 µm, probably the result of vapor-phase crystallization. One pantellerite (sample 007a) contains a spherule of crystal-rich material (<100 µm diameter) that includes quartz microcrystals.

INTENSIVE PARAMETERS

We used a variety of techniques to constrain the conditions under which differentiation occurred.

Temperature

Pre-eruption temperatures were calculated utilizing the available mineral compositions; both single- and multiple-mineral methods and mineral/glass (liquid) thermometers are detailed next. Peralkaline rocks, in particular, contain limited phenocrysts and are usually lacking in the mineral assemblages suitable for thermobarometry, making temperature estimation notoriously difficult. However, by calculating temperatures via several methodologies, it has been possible to build a comprehensive picture of pre-eruption temperatures across all rock types (supplementary Table 11 [see footnote 1]).

Fe-Ti–Oxide Thermometry

Coexisting Fe-Ti oxides are limited in the Dabbahu samples; usually one of the oxides will dominate, with just one or two crystals of the other present, and touching Fe-Ti–oxide pairs were only found in two samples. The program ILMAT (Lepage, 2003) was used to calculate the FeO/Fe_2O_3 ratio with the method of Carmichael (1967), and to check stoichiometry. Each ilmenite was then checked against each magnetite analysis in the same sample for Mg/Mn equilibrium following Bacon and Hirschmann (1988). Data that failed this test were excluded. Although not ideal, due to the rarity of oxide pairs, individual analyses were used. Averaging the oxides from a sample was not carried out, as this would introduce uncertainty as to whether all ilmenites were in equilibrium with all magnetites, and it would also hide any significant trends or temporal evolution within an individual sample (Blundy and Cashman, 2008). Each equilibrium pair was then processed using the method of Ghiorso and Evans (2008) to determine temperature and oxygen fugacity (Fig. 9).

Thirteen samples yielded temperatures from Fe-Ti oxides, four of which were rhyolites, the rest being intermediate samples (basaltic trachyandesite, trachyandesite, and trachyte; supplemental Table 9 [see footnote 1]; Fig. 9). Temperatures range from 716 to 997 °C in the rhyolites, and 919–1168 °C in the intermediates. Bizouard et al. (1980) obtained three temperatures from intermediate samples using Fe-Ti oxides: 930 °C, 990 °C, and 1010 °C. However, recalculation of these temperatures using the same methods as for our samples showed only one sample to have oxides in equilibrium, yielding a revised temperature of 992 °C, which is in line with temperatures obtained from the current

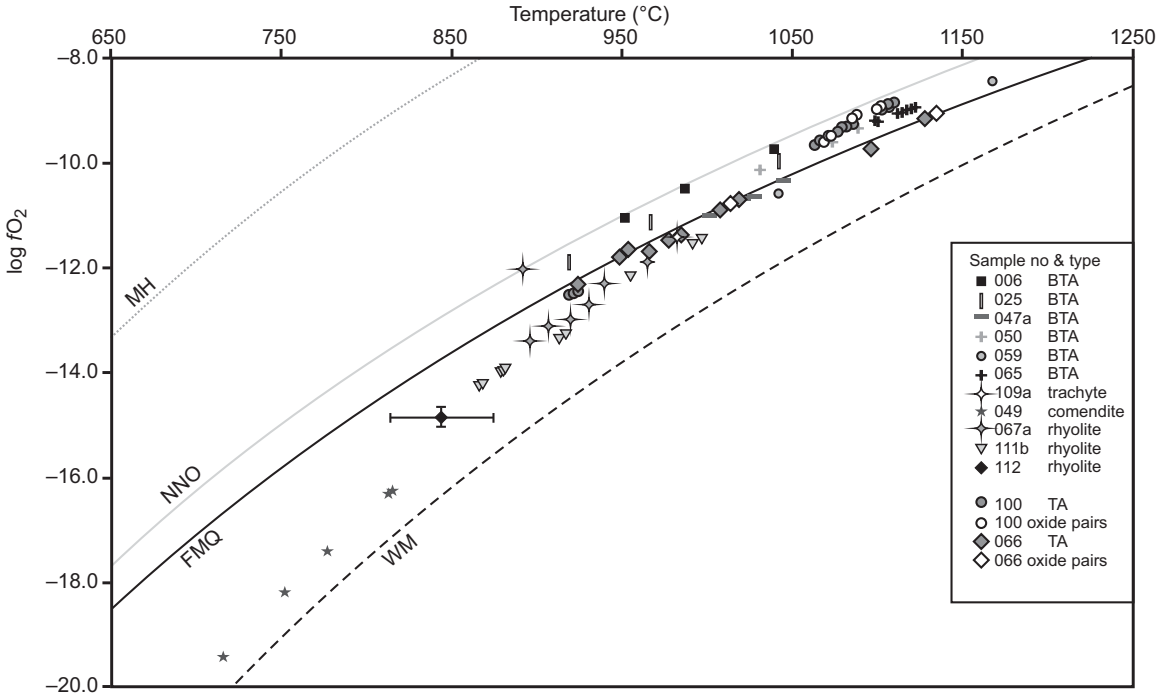

Figure 9. Temperature vs. oxygen fugacity from Fe-Ti oxides calculated using the method of Ghiorso and Evans (2008). Two samples (100 and 066) contain touching oxide pairs, indicated by an open circle and diamond, respectively. The touching oxide pairs correspond to the range shown by nontouching pairs within each sample. Buffers were calculated from Frost (1991). MH—magnetite-hematite, NNO—nickel-nickel oxide, FMQ—fayalite-magnetite-quartz, WM—wüstite-magnetite, BTA—basaltic trachyandesite, TA—trachyandesite. An error bar indicating the typical standard error of estimate (SEE) error is shown.

study for intermediate rocks. One trachyandesite (sample 100) shows two distinct temperature groupings of 920–924 °C and 1063–1110 °C, suggestive of magma mixing immediately prior to eruption, i.e., without sufficient time for re-equilibration. Two samples contained oxide pairs (066 and 100), and the temperatures obtained through these pairs correspond to the temperatures gained from the individual oxides.

Feldspar-Liquid Thermometry

Feldspar is the main phenocryst phase in the rhyolites of Dabbahu. Because the majority of rhyolites are obsidians, the "liquid" composition can be obtained from analyses of the coexisting glass. Plagioclase-liquid thermometry was also used for nine samples. Electron microprobe data from matrix glasses and feldspars (alkali feldspar and plagioclase) were used to calculate the temperature using the method of Putirka (2008). Two-feldspar thermometry was not utilized as the feldspars were deemed texturally unsuitable (e.g., plagioclase phenocrysts coexisting with alkali feldspar groundmass).

Alkali Feldspar-Liquid

Temperatures were obtained from 27 rhyolite samples using the alkali feldspar-liquid thermometer (Putirka, 2008; supplementary Table 11 [see footnote 1]). The total range of calculated temperatures is 686–887 °C with a standard error of estimate (SEE) of ±23 °C. In all but four samples, the range of temperatures is <10 °C.

Plagioclase-Liquid

Five metaluminous rhyolites, three intermediates (basaltic trachyandesite, trachyandesite, and trachyte), and a comendite sample yielded temperatures using the plagioclase-liquid thermometer (Putirka, 2008). The calculated temperature range for rhyolites is higher than given by the alkali feldspar-liquid thermometer at 885–1080 °C, with a SEE ±36 °C; individual samples have ranges spanning <14 °C. The range within the intermediate samples (848–983 °C) is lower than the rhyolite range.

Clinopyroxene-Liquid Thermometry

Clinopyroxene phenocrysts are found throughout the Dabbahu samples; however, it is often difficult to analyze the "liquid" phase, and therefore the (phenocryst-poor) whole-rock composition has been utilized as representative of a nominal liquid. Clinopyroxene thermometry is sensitive to pressure, which can be calculated from clinopyroxene and liquid composition by solving pressure-temperature (*P-T*) equations simultaneously. The clinopyroxene and coexisting "liquid" were checked for equilibrium by using predicted and observed values for clinopyroxene components (e.g., DiHd, EnFs, etc.), and any data shown not to be in equilibrium were rejected (Putirka, 2008). This method was used in preference to Fe-Mg exchange because it has been shown to be more robust (Putirka, 2008), especially as Dabbahu clinopyroxenes are generally very low in Mg. Temperatures were calculated using the Jd-DiHd exchange thermometer (Putirka, 2008). In many of the rhyolites, it was not possible to calculate pressures from the clinopyroxene because of the probably relatively shallow magma storage region below Dabbahu; based on melt inclusion volatile-saturation pressures, Field et al. (2012b) estimated the magma storage region beneath Dabbahu to lie at <5 km.

Application of the clinopyroxene-liquid thermometer on 21 samples yielded a total range of 894–1205 °C, SEE ±45 °C (supplementary Table 11 [see footnote 1]). Temperatures were derived from clinopyroxene from all rock types except rhyolites. The most primitive phenocryst-bearing basalt (044) yielded the highest temperature range of 1171–1205 °C. Where temperatures were derived from both Fe-Ti oxides and clinopyroxene-liquid for the same samples, these are generally consistent: e.g., in sample 047a, Fe-Ti oxides give a temperature range of 1001–1045 °C, and clinopyroxene-liquid gives a range of 1005–1039 °C.

Olivine-Liquid Thermometry

Olivine-liquid thermometry was used to investigate temperatures for the basalts. As for clinopyroxene, whole rock was utilized as representative of a nominal liquid. The phenocrysts were checked for equilibrium with the whole rock using the method of Roeder (1974). Only two phenocrysts from sample 103 passed the equilibrium test (Kd [Fe-Mg] ol-liq = 0.30 ± 0.03). The calculated temperatures (1113 and 1117 °C, SEE ±53 °C) show a close match to the calculated clinopyroxene-liquid temperatures.

Temperature Summary

The temperatures calculated by the different methods are broadly consistent with differentiation from basalts (≥1250 °C) to rhyolites (~680 °C). Although temperature generally decreases with increasing SiO_2, some samples show indications of bimodal temperatures, particularly trachyandesite sample 100, which has two distinct groupings separated by a temperature gap of ~150 °C. This supports the hypothesis of magma mixing just prior to eruption, where insufficient time passed to allow the oxides to re-equilibrate to the new conditions, thus preserving the original temperature signature of the two melts involved.

The alkali feldspar-liquid temperatures derived for the peralkaline rhyolites were 686–887 °C. This range lies at the upper end of the published temperature estimates for other peralkaline rocks, e.g., Olkaria obsidians (NK/A = 1.01–1.55) 660–740 °C (Marshall et al., 2009); Eburru complex (NK/A = 1.11–2.2) trachytes 709–793 °C and pantellerites 668–708 °C (Ren et al., 2006); Pantelleria Green Tuff (NK/A = 1.07–1.97) 703–944 °C (White et al., 2009). It is possible that this is related to the relatively mild peralkalinity of the Dabbahu samples or differing H_2O contents. The Dabbahu samples do not have the same mineral assemblage as these other examples, in which, for example, quartz is an essential phenocryst. Available temperature data for peralkaline rhyolites are also very limited due to the difficulties in deriving temperatures from such a limited mineral assemblage. There is no clear correlation in the samples of this study between NK/A and temperature. The narrow temperature range within each sample derived from alkali feldspar thermometry reflects the narrow compositional range of feldspars found in the Dabbahu peralkaline rocks.

Clinopyroxene-liquid and olivine-liquid thermometry provides temperatures for the Dabbahu basalts. Basalt sample 044 yielded the highest temperatures of any of the samples (1171–1205 °C). This is lower than the 1275 °C obtained by Bizouard et al. (1980) for one Dabbahu basalt based on olivine composition and Fe^{2+}/Mg ratio. Some samples have significantly larger temperature ranges, which can be ascribed to magma mixing, which is suggested by textural evidence in some samples. Clinopyroxene-liquid and olivine-liquid temperatures calculated for sample 103 closely correspond. Fe-Ti–oxide temperatures calculated for intermediate samples complement temperatures calculated using clinopyroxene-liquid thermometry.

Oxygen Fugacity

Oxygen fugacity (fO_2) was determined using Fe-Ti–oxide equilibria following the same procedure as for temperature (supplementary Table 11 [see footnote 1]). Each equilibrium pair was processed using the method of Ghiorso and Evans (2008) and calculated as log units relative to the FMQ buffer (Fig. 9).

When viewed as a whole, the data show a broad range of $\log fO_2$ equilibrium conditions in relation to the FMQ buffer (–3.6 to +0.5) without any significant trends. However, the lowest fO_2 is recorded by the most-evolved rock

evaluated here (sample 049, a comendite). The samples from this study are broadly consistent with data for similar rocks from the literature recalculated using the same methodology. White et al. (2005) concluded that the redox state of natural peralkaline and cogenetic high-alkali metaluminous rock is consistently near or below the FMQ buffer for a temperature range of 1025 °C to 685 °C, a conclusion entirely in keeping with data from Dabbahu.

MAGMATIC EVOLUTION AT DABBAHU

Constraining the pressure (depth) at which differentiation occurred is not possible using conventional geobarometers (see previous), because these do not provide the requisite accuracy at low pressure. Melt inclusions (Field et al., 2012b) indicate volatile saturation pressures of 47–203 MPa. Further constraints can be obtained from experimental studies. There have been no published experimental investigations of Dabbahu basalts, although the experiments of Whitaker et al. (2008, 2007), aimed at investigating magma differentiation in the Snake River Plain (USA), utilized an olivine tholeiite starting material that is a remarkably close match to likely parental basalt compositions at Dabbahu. Whitaker et al.'s (2007, 2008) experiments were carried out at a variety of pressures, and with low H_2O contents (0.05–0.4 wt% H_2O) to simulate basalt differentiation in the middle to shallow crust. A suite of experiments at 430 MPa with 0.4 wt% H_2O was run to simulate fractional crystallization by synthesizing a residual trachybasalt glass from higher-temperature experiments and using it as starting material for lower-temperature experiments.

Plotting Whitaker et al.'s (2007, 2008) experimental liquid compositions alongside our Dabbahu whole-rock analyses (Fig. 10) sheds considerable light on crystallization conditions. For pressures at and above 630 MPa, crystallization drives liquids initially to lower SiO_2, at odds with the whole-rock trend at Dabbahu. At lower pressures, SiO_2 enrichment is observed. The closest match between experiments and Dabbahu whole rocks is for the experiments at 430 MPa and initial bulk water content of 0.4 wt%. These experiments not only reproduce the observed SiO_2 enrichment, but also peaks in TiO_2, FeO, and P_2O_5, corresponding to saturation with oxides and apatite, and the marked kinks in the MgO and CaO trends (Fig. 10). Only the alkalis do not provide an excellent match between experiments and whole rocks (see following).

The experimental H_2O content is reasonable for parental basalts at Dabbahu. Pantellerites contain melt inclusions with H_2O contents of up to 5.8 wt% (Field et al., 2012b). Assuming between 80% and 90% crystallization (closed-system fractionation and perfect incompatibility of water), this can be back-calculated to give parent basalt H_2O contents of between 0.6 and 1 wt%. These are lower bounds, because they assume that the pantellerites are at the point of H_2O saturation and have not degassed significantly. The liquidus temperature of Snake River Plain tholeiite with 0.4 wt% H_2O is 1220 °C (Whitaker et al., 2008), in good agreement with our temperature estimates for basalts given herein. Whitaker et al. (2008) pointed out that alkali feldspar was absent from the experimental assemblages, and the experiments failed to produce the most-evolved liquids of the natural suites at Snake River Plain, yielding a slight depletion in Na_2O and enrichment in K_2O values compared to the natural data (also seen in comparison to the Dabbahu data; Fig. 10). They suggested this may be the result of a lack of fluorine in the experiments. Analyses of melt inclusions at Dabbahu (Field et al., 2012b) have identified the presence of fluorine, but although halogens can be extremely elevated in pantellerites (e.g., Lowenstern, 1994), the values found in Dabbahu melt inclusions are not exceptional (F <3000 ppm and Cl <3100 ppm).

Fractional crystallization of parental basalts has long been argued as a feasible method of producing peralkaline rocks, both at Dabbahu and elsewhere in the African Rift (e.g., Barberi et al., 1974b; Marshall et al., 2009). Evidence from geochemistry (Fig. 7) and experiments (Fig. 10) supports this hypothesis. Basalts such as those recently erupted in the Manda-Hararo rift segment represent plausible parents for the differentiation sequence at Dabbahu. The H_2O content of these basalts is likely to have been low (<1 wt%), consistent with recent analysis of olivine-hosted melt inclusions from recent basalts at Erta'Ale volcano to the north (Field et al., 2012a) and the inferences from experimental work (see previous). Closed-system differentiation of such basalts would have generated rhyolites with the elevated H_2O contents observed in melt inclusions (Field et al., 2012b). Continuous, protracted fractionation is suggested by the smooth variations in mineral compositions from basalt to rhyolite. Simple mass-balance calculations indicate that ~70% crystallization is required to reach pantellerite composition from a parental basalt, and a higher percent crystallization would be required to reach the composition of the most-evolved aphyric samples (see supplementary Table 12 [see footnote 1]). We note that the most evolved melts in the Whitaker et al. (2008) fractional crystallization experiments have 69 wt% SiO_2 (Fig. 10) and correspond to a total crystallization of 93 wt% from their olivine tholeiite parent.

It is notable that the phenocryst assemblage olivine + clinopyroxene + feldspar is stable across the entire compositional range, consistent with fractionation at relatively low fO_2. More oxidized conditions would lead to the formation of orthopyroxene via peritectic reaction of olivine with melt (Frost and Lindsley, 1992), yet orthopyroxene is not observed in any rock sample from Dabbahu. In the 430 MPa experiments of Whitaker et al. (2008), which were carried out in graphite capsules at estimated fO_2 2–3 log units below FMQ, also crystallize olivine + clinopyroxene + feldspar from 1220 °C to 960 °C; pigeonite, which is absent at Dabbahu, appears at 940 °C. Low fO_2 is also consistent with the occurrence of aenigmatite.

Although the majority of Dabbahu rocks are crystal-poor and therefore represent likely liquid compositions, there is considerable textural and mineralogical evidence of magma mixing between more- and less-evolved melts. On the basis of mineralogical and major-element chemical variations alone, we cannot rule out some assimilation of older crustal rocks during differentiation. Indeed, there is textural evidence presented here for entrainment of granitic plutonic rock fragments in a few samples. However, the chemical and mineralogical trends, coupled with the absence of any prominent compositional gap, and the close correspondence to the experiments of Whitaker et al. (2008) argue for protracted fractional crystallization as the dominant differentiation mechanism from basalt to rhyolite. The experimental conditions suggest that fractionation occurred close to 420 MPa, representing differentiation at midcrustal levels (12–16 km). This pressure (depth) is consistent with the high end of the range of melt inclusion volatile saturation pressures recorded by Field et al. (2012b).

It is clear that the plumbing system beneath Dabbahu enabled the eruption of a wide variety of cogenetic magma types over a short time interval (Fig. 5). This may be because differentiation must have taken place on time scales that are shorter than the overall age of the volcano (ca. 67 ka). This is consistent with differentiation of relatively small magma bodies within the crust such that the cooling rate of basalts, and consequent crystallization, is rapid. Such an idea is in keeping with the findings of Lowenstern et al. (2006), who calculated ~50–60 k.y. from mantle extraction to granite formation for the Alid volcanic system in Eritrea using U-Th disequilibrium and dating of zircons. Alternatively, the magmatic system beneath Dabbahu may be large, but sufficiently stratified compositionally and temporally that magmas of different composition can be effectively isolated from each other for the lifetime of the volcano. The

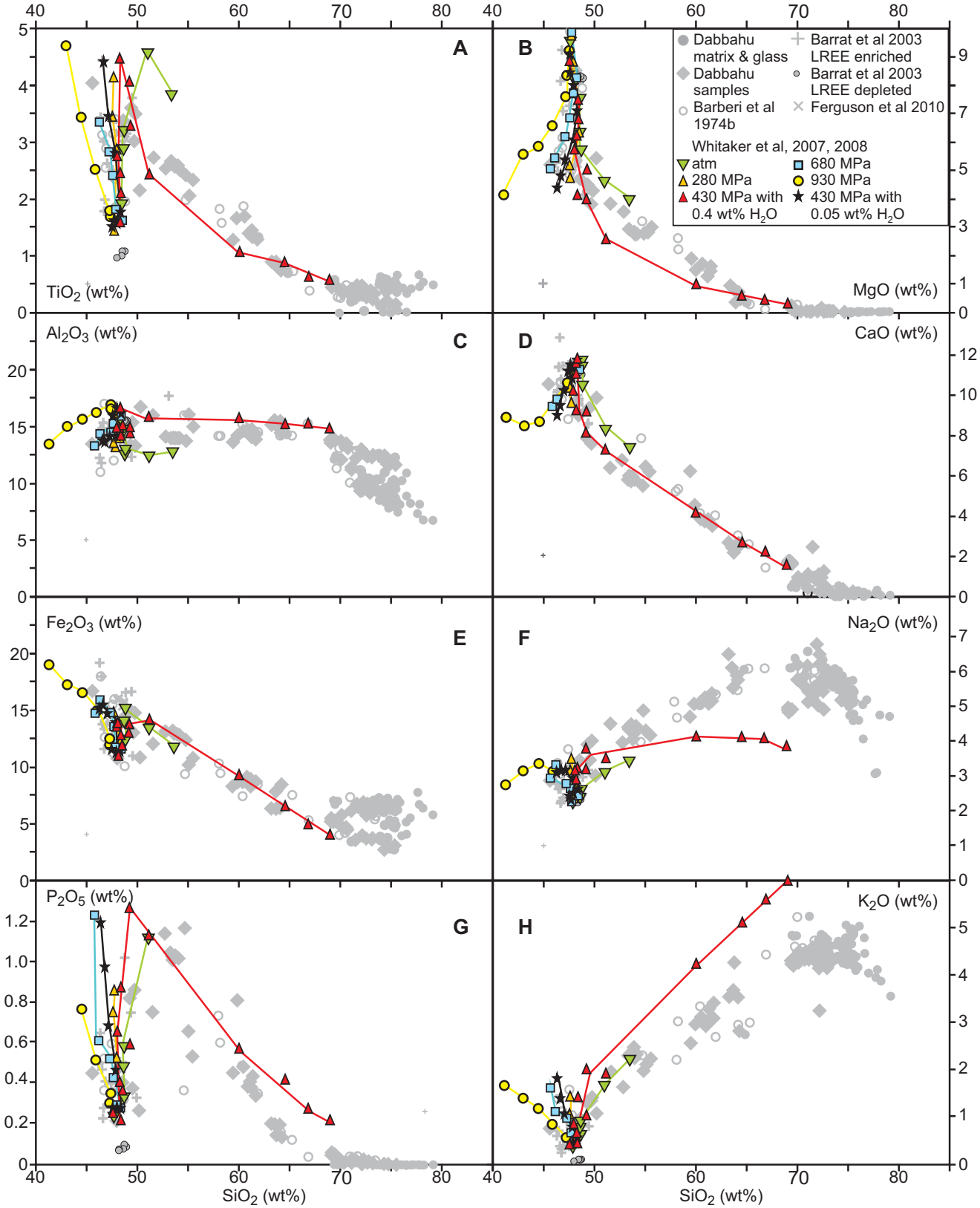

Figure 10. Selected major element vs. SiO_2 Harker diagrams for experimental glasses from Whitaker et al. (2007, 2008) compared to whole-rock data from Dabbahu. The experiments at 430 MPa with 0.4 bulk wt% H_2O show a close match to the Dabbahu samples, with the exception of Na_2O, which is depleted compared to Dabbahu samples, and K_2O, which is enriched. The anhydrous experiments, particularly those at pressures of >680 MPa, describe trends of decreasing SiO_2 with differentiation at odds with the whole-rock data. LREE—light rare earth element.

volcanic load of Dabbahu may have served as an effective mechanism (Pinel and Jaupart, 2000) to focus such a diversity of magma composition through a series of closely spaced vents or fissures. Whatever the details of the sub-Dabbahu plumbing system, the largely aphyric nature of most of the evolved Dabbahu samples argues for very efficient melt-solid segregation.

Geochronology and field evidence (Fig. 5) suggest a possible hiatus in eruptive activity between the youngest comenditic lavas and the more-evolved pantellerites. The youngest comendites were dated at 30.1 ± 0.4 ka and 28.6 ± 0.7 ka. The oldest pantellerites, those that are pumice-covered to the N and NW of the summit, erupted around 7.8 ± 4.3 ka. This may in part be a result of a sampling bias (for example, it is not currently possible to reach the eastern side of Dabbahu), and future work may provide samples that fill in this gap. However, we also suggest that the hiatus of ~16 k.y. may give an indication of the time span required to fractionate the pantellerite liquids at Dabbahu. Most of the pantellerite rocks have also been erupted from fissure systems, whereas the comenditic lavas have been erupted as individual flows from single vents, suggesting there may have been subtle changes in eruptive style and/or magma plumbing during this time.

CONCLUSIONS

Dabbahu volcano reveals a complex magmatic history. It originated as a basaltic shield volcano, and approximately coeval to the formation, a metaluminous rhyolite complex formed. New ^{40}Ar-^{39}Ar dating indicates the formation of Dabbahu began prior to 67 ka and has continued to the present. Over its history, the volcano has erupted a wide variety of magma types from transitional basalt through trachyte to peralkaline rhyolites (pantellerites and rhyolites) from a relatively tightly spaced distribution of vents and fissures. New field evidence confirms that these products were not erupted in order of increasing silica content, in contrast to the original proposal of Barberi et al. (1974b).

Erupted rocks are generally poor in phenocrysts, making them likely candidates for true liquid compositions, little modified by crystal entrainment or accumulation. Mineral compositions show continuous and extreme variation across the range in rock types, with the assemblage olivine + clinopyroxene + feldspar ubiquitous. Olivine, for example ranges in composition from Fo_{84} in basalts to Fo_0 in rhyolites. The calculated temperature range (~1200–680 °C), provides a guide to the pre-eruptive temperatures at Dabbahu, which is in line with expected temperatures for the rock types found. The magmas were relatively reduced (fO_2 at or close to FMQ buffer), consistent with the lack of orthopyroxene from any sample studied and the presence of aenigmatite. The parental basalts contained <1 wt% H_2O, but protracted fractionation enabled considerable enrichment in H_2O of the most-evolved rocks, leading to occasional explosive, as well as effusive, eruptions.

Comparison to experimental work on similar rock types suggests the key petrogenetic process is likely to be fractional crystallization of rift-related basalts at midcrustal depths, ~10–15 km. Direct experiments on Dabbahu compositions are required to confirm this assertion. The relatively short time scales of differentiation, relative to the age of the edifice, and the lack of temporal progression argue for rapid cooling of parental basalts, either due to the relatively small size of the differentiating bodies or to their relatively shallow depth. There is conclusive evidence of mixing between different, cogenetic magmas recorded at Dabbahu on all scales, from macro- to microscale. Mixing is likely to have occurred either shortly prior to eruption or syneruptively. The subvolcanic plumbing system at Dabbahu enabled coexistence of cogenetic magmas of contrasted composition, rather than a single large magma chamber, in which it is hard to envisage the coexistence of such diverse liquids over such a short time span. A series of stacked sills or closely spaced dikes distributed throughout the subvolcanic region may have provided the necessary configuration. Such a proposal is consistent with evidence from melt inclusions, seismology, and geodesy (Field et al., 2012b). The recent eruption of rhyolite from the Da'Ure vent to the east of Dabbahu following a period of basalt dike injection (Wright et al., 2006) suggests that influx of new magmas into the subvolcanic magma storage region may have acted as a key eruptive trigger throughout the volcano's history.

ACKNOWLEDGMENTS

We would like to thank C. Bacon, J. Lowenstern, J. Maclennan, and C. Miller for insightful and constructive reviews of this manuscript. This work has been supported by National Environmental Research Council Afar Rift Consortium grant NE/F007604/1. We acknowledge the generous support of the University of Addis Ababa with field-work arrangements, particularly E. Lewi and A. Ayele, and the Afar Regional Government for invaluable assistance. We gratefully acknowledge technical assistance provided by S. Kearns (electron microprobe), N. Marsh, and R. Kelly (X-ray fluorescence).

REFERENCES CITED

Acocella, V., 2010, Coupling volcanism and tectonics along divergent plate boundaries: Collapsed rifts from central Afar, Ethiopia: Geological Society of America Bulletin, v. 122, p. 1717–1728, doi:10.1130/B30105.1.

Acocella, V., Korme, T., Salvini, F., and Funiciello., R., 2002, Elliptic calderas in the Ethiopian Rift: Control of pre-existing structures: Journal of Volcanology and Geothermal Research, v. 119, p. 189–203, doi:10.1016/S0377-0273(02)00342-6.

Acocella, V., Abebe, B., Korme, T., and Barberi, F., 2008, Structure of Tendaho graben and Manda Hararo rift: Implications for the evolution of the southern Red Sea propagator in Central Afar: Tectonics, v. 27, TC4016, doi:10.1029/2007TC002236.

Ayele, A., Jacques, E., Kassim, M., Kidane, T., Omar, A., Tait, S., Nercessian, A., de Chabalier, J., and King, G., 2007, The volcano-seismic crisis in Afar, Ethiopia, starting September 2005: Earth and Planetary Science Letters, v. 255, p. 177–187, doi:10.1016/j.epsl.2006.12.014.

Bacon, C.R., and Hirschmann, M.M., 1988, Mg/Mn partitioning as a test for equilibrium between co-existing Fe-Ti oxides: The American Mineralogist, v. 73, p. 57–61.

Barberi, F., and Varet, J., 1977, Volcanism of Afar—Small-scale plate tectonic implications: Geological Society of America Bulletin, v. 88, p. 1251–1266, doi:10.1130/0016-7606(1977)88<1251:VOASPT>2.0.CO;2.

Barberi, F., Tazieff, H., and Varet, J., 1972, Volcanism in the Afar Depression: Its tectonic and magmatic significance: Tectonophysics, v. 15, p. 19–29, doi:10.1016/0040-1951(72)90046-7.

Barberi, F., Bonatti, E., Marinelli, G., and Varet, J., 1974a, Transverse tectonics during the split of a continent: Data from the Afar Rift: Tectonophysics, v. 23, p. 17–29, doi:10.1016/0040-1951(74)90108-5.

Barberi, F., Ferrara, R., Santacroce, R., Treuil, M., and Varet, J., 1974b, A transitional basalt—Pantellerite sequence of fractional crystallisation, the Boina centre, (Afar Rift, Ethiopia): Journal of Petrology, v. 16, p. 22–56.

Barberi, F., Santacroce, R., and Varet, J., 1974c, Silicic peralkaline volcanic rocks of the Afar Depression (Ethiopia): Bulletin Volcanologique, v. 38, p. 755–790, doi:10.1007/BF02596907.

Barrat, J.A., Joron, J.L., Taylor, R.N., Fourcade, S., Nesbitt, R.W., and Jahn, B.M., 2003, Geochemistry of basalts from Manda Hararo, Ethiopia: LREE-depleted basalts in Central Afar: Lithos, v. 69, p. 1–13, doi:10.1016/S0024-4937(03)00044-6.

Beutel, E., van Wijk, J., Ebinger, C., Keir, D., and Agostini, A., 2010, Formation and stability of magmatic segments in the Main Ethiopian and Afar Rifts: Earth and Planetary Science Letters, v. 293, p. 225–235, doi:10.1016/j.epsl.2010.02.006.

Bizouard, H., Barberi, F., and Varet, J., 1980, Mineralogy and petrology of Erta Ale and Boina volcanic series, Afar Rift, Ethiopia: Journal of Petrology, v. 21, p. 401–436.

Blundy, J., and Cashman, K., 2008, Petrologic reconstruction of magmatic system variables and processes, *in* Putirka, K.D., and Tepley, F.J., III, eds., Minerals, Inclusions and Volcanic Processes: Mineralogical Society of America Reviews in Mineralogy and Geochemistry, v. 69, p. 179–239.

Brinckmann, J., and Kuersten, M., 1970, Geologische Uebersichtskarte der Danakil-Senke (Geological Sketch Map of the Danakil Depression): Hanover, Germany, Bundesanstalt für Bodenforschung, Federal Republic of Germany, scale 1:250,000.

Carmichael, I.S.E., 1966, The iron-titanium oxides of salic volcanic rocks and their associated ferromagnesian silicates: Contributions to Mineralogy and Petrology, v. 14, p. 36–64, doi:10.1007/BF00370985.

Chu, D.Z., and Gordon, R.G., 1998, Current plate motions across the Red Sea: Geophysical Journal International, v. 135, p. 313–328, doi:10.1046/j.1365-246X.1998.00658.x.

Chu, D.Z., and Gordon, R.G., 1999, Evidence for motion between Nubia and Somalia along the Southwest Indian Ridge: Nature, v. 398, p. 64–67, doi:10.1038/18014.

Di Carlo, I., Rotolo, S.G., Scaillet, B., Buccheri, V., and Pichavant, M., 2010, Phase equilibrium constraints on pre-eruptive conditions of recent felsic explosive volcanism at Pantelleria Island, Italy: Journal of Petrology, v. 51, p. 2245–2276, doi:10.1093/petrology/egq055.

Ebinger, C., Ayele, A., Keir, D., Rowland, J., Yirgu, G., Wright, T., Belachew, M., and Hamling, I., 2010, Length and timescales of rift faulting and magma intrusion: The Afar rifting cycle from 2005 to present: Annual Review of Earth and Planetary Sciences, v. 38, p. 439–466.

Ernst, W.G., 1962, Synthesis, stability relations, and occurrence of riebeckite and riebeckite-arfvedsonite solid solutions: The Journal of Geology, v. 70, p. 689–736.

Esser, R.P., Kyle, P.R., and McIntosh, W.C., 2004, $^{40}Ar/^{39}Ar$ dating of the eruptive history of Mount Erebus, Antarctica: Volcano evolution: Bulletin of Volcanology, v. 66, p. 671–686, doi:10.1007/s00445-004-0354-x.

Ferguson, D.J., Barnie, T.D., Pyle, D.M., Oppenheimer, C., Yirgu, G., Lewi, E., Kidane, T., Carn, S., and Hamling, I., 2010, Recent rift-related volcanism in Afar, Ethiopia: Earth and Planetary Science Letters, v. 292, p. 409–418, doi:10.1016/j.epsl.2010.02.010.

Field, L., Barnie, T., Blundy, J., Brooker, R.A., Keir, D., Lewi, E., and Saunders, K., 2012a, Integrated field, satellite and petrological observations of the November 2010 eruption of Erta Ale: Bulletin of Volcanology, doi:10.1007/s00445-012-0660-7 (in press).

Field, L., Blundy, J., Brooker, R.A., Wright, T., and Yirgu, G., 2012b, Magma storage conditions beneath Dabbahu Volcano (Ethiopia) constrained by petrology, seismicity and satellite geodesy: Bulletin of Volcanology, v. 74, p. 981–1004, doi:10.1007/s00445-012-0580-6.

Frost, B.R., 1991, Introduction to oxygen fugacity and its petrologic importance: Reviews in Mineralogy and Geochemistry, v. 25, no. 1, p. 1–9.

Frost, B.R., and Lindsley, D.H., 1992, Equilibria among Fe-Ti oxides, pyroxenes, olivine and quartz: 2. Application: The American Mineralogist, v. 77, p. 1004–1020.

Ghiorso, M.S., and Evans, B.W., 2008, Thermodynamics of rhombohedral oxide solid solutions and a revision of the Fe-Ti two-oxide geothermometer and oxygen-barometer: American Journal of Science, v. 308, p. 957–1039, doi:10.2475/09.2008.01.

Gibson, I.L., 1970, A pantelleritic welded ash-flow tuff from the Ethiopian Rift Valley: Contributions to Mineralogy and Petrology, v. 28, p. 89–111, doi:10.1007/BF00404992.

Grew, E.S., Halenius, U., Pasero, M., and Barbier, J., 2008, Recommended nomenclature for the sapphirine and surinamite groups (sapphirine supergroup): Mineralogical Magazine, v. 72, p. 839–876, doi:10.1180/minmag.2008.072.4.839.

Hamling, I.J., Ayele, A., Bennati, L., Calais, E., Ebinger, C.J., Keir, D., Lewi, E., Wright, T.J., and Yirgu, G., 2009, Geodetic observations of the ongoing Dabbahu rifting episode: New dyke intrusions in 2006 and 2007: Geophysical Journal International, v. 178, p. 989–1003, doi:10.1111/j.1365-246X.2009.04163.x.

Hamling, I.J., Wright, T.J., Calais, E., Bennati, L., and Lewi, E., 2010, Stress transfer between thirteen successive dyke intrusions in Ethiopia: Nature Geoscience, v. 3, p. 713–717, doi:10.1038/ngeo967.

Hayward, N.J., and Ebinger, C.J., 1996, Variations in the along-axis segmentation of the Afar Rift system: Tectonics, v. 15, p. 244–257, doi:10.1029/95TC02292.

Irvine, T.N., and Baragar, W.R.A., 1971, A guide to the chemical classification of the common volcanic rocks: Canadian Journal of Earth Sciences, v. 8, p. 523–548, doi:10.1139/e71-055.

Kuno, H., 1960, High-alumina basalt: Journal of Petrology, v. 1, p. 121–145, doi:10.1093/petrology/1.1.121.

Kunzmann, T., 1999, The aenigmatite-rhonite mineral group: European Journal of Mineralogy, v. 11, p. 743–756.

Lahitte, P., Gillot, P., and Courtillot, V., 2003a, Silicic central volcanoes as precursors to rift propagation; the Afar case: Earth and Planetary Science Letters, v. 207, p. 103–116, doi:10.1016/S0012-821X(02)01130-5.

Lahitte, P., Gillot, P.Y., Kidane, T., Courtillot, V., and Bekele, A., 2003b, New age constraints on the timing of volcanism in Central Afar, in the presence of propagating rifts: Journal of Geophysical Research–Solid Earth, v. 108, 2123, doi:10.1029/2001JB001689.

Le Maitre, R.W., 2002, Igneous Rocks: A Classification and Glossary of Terms. Recommendations of the International Union of Geological Sciences Subcommission on the Systematics of Igneous Rocks: Cambridge, UK, Cambridge University Press, 256 p.

Lepage, L.D., 2003, ILMAT: An Excel worksheet for ilmenite-magnetite geothermometry and geobarometry: Computers & Geosciences, v. 29, p. 673–678, doi:10.1016/S0098-3004(03)00042-6.

Lowenstern, J.B., 1994, Chlorine, fluid immiscibility and degassing in peralkaline magmas from Pantelleria, Italy: The American Mineralogist, v. 79, p. 353–369.

Lowenstern, J.B., Charlier, B.L.A., Clynne, M.A., and Wooden, J.L., 2006, Extreme U-Th disequilibrium in rift-related basalts, rhyolites and granophyric granite and the time scale of rhyolite generation, intrusion and crystallization at Alid volcanic center, Eritrea: Journal of Petrology, v. 47, p. 2105–2122, doi:10.1093/petrology/egl038.

MacDonald, GA., 1968, Composition and origin of Hawaiian lavas, *in*, Coats, R.R., Hay, R.L., and Anderson, C.A., eds., Studies in Volcanology: A Memoir in Honor of Howel Williams: Geological Society of America Memoir 116, p. 477–522.

Macdonald, R., 1974, Nomenclature and petrochemistry of the peralkaline oversaturated extrusive rocks: Bulletin Volcanologique, v. 38, p. 498–516, doi:10.1007/BF02596896.

Macdonald, R., and Bailey, D.K., 1973, Chemistry of igneous rocks: Part 1. The chemistry of the peralkaline oversaturated obsidians, *in* Fleischer, M., ed., Data of Geochemistry: U.S. Geological Survey Professional Paper 440, p. 37.

Manighetti, I., Tapponnier, P., Courtillot, V., Gruszow, S., and Gillot, P.Y., 1997, Propagation of rifting along the Arabia-Somalia plate boundary: The Gulfs of Aden and Tadjoura: Journal of Geophysical Research–Solid Earth, v. 102, p. 2681–2710, doi:10.1029/96JB01185.

Marshall, A.S., Macdonald, R., Rogers, N.W., Fitton, J.G., Tindle, A.G., Nejbert, K., and Hinton, R.W., 2009, Fractionation of peralkaline silicic magmas: The Greater Olkaria volcanic complex, Kenya Rift Valley: Journal of Petrology, v. 50, p. 323–359, doi:10.1093/petrology/egp001.

Marshall, L.A., and Sparks, R.S.J., 1984, Origin of some mixed-magma and net-veined ring intrusions: Journal of the Geological Society of London, v. 141, p. 171–182, doi:10.1144/gsjgs.141.1.0171.

McKenzie, D.P., Davies, D., and Molnar, P., 1970, Plate tectonics of the Red Sea and East Africa: Nature, v. 226, p. 243, doi:10.1038/226243a0.

Noble, D.C., 1968, Systematic variation of major elements in comendite and pantellerite glasses: Earth and Planetary Science Letters, v. 4, p. 167–172, doi:10.1016/0012-821X(68)90011-3.

Pinel, V., and Jaupart, C., 2000, The effect of edifice load on magma ascent beneath a volcano: Philosophical Transactions of the Royal Society of London, ser. A, Mathematical, Physical and Engineering Sciences, v. 358, p. 1515–1532, doi:10.1098/rsta.2000.0601.

Prodehl, C., Fuchs, K., and Mechie, J., 1997, Seismic-refraction studies of the Afro-Arabian rift system—A brief review: Tectonophysics, v. 278, p. 1–13, doi:10.1016/S0040-1951(97)00091-7.

Putirka, K.D., 2008, Thermometers and barometers for volcanic systems: Minerals, inclusions and volcanic processes: Reviews in Mineralogy and Geochemistry, v. 69, p. 61–120, doi:10.2138/rmg.2008.69.3.

Ren, M., Omenda, P.A., Anthony, E.Y., White, J.C., Macdonald, R., and Bailey, D.K., 2006, Application of the QUILF thermobarometer to the peralkaline trachytes and pantellerites of the Eburru volcanic complex, East African Rift: Kenya: Lithos, v. 91, p. 109–124.

Roeder, P.L., 1974, Activity of iron and olivine solubility in basaltic liquids: Earth and Planetary Science Letters, v. 23, p. 397–410.

Rowland, J., Baker, E., Ebinger, C., Keir, D., Kidane, T., Biggs, J., Hayward, N., and Wright, T.J., 2007, Fault growth at a nascent slow-spreading ridge: 2005 Dabbahu rifting episode, Afar: Geophysical Journal International, v. 171, p. 1226–1246, doi:10.1111/j.1365-246X.2007.03584.x.

Scaillet, B., and Macdonald, R., 2001, Phase relations of peralkaline silicic magmas and petrogenetic implications: Journal of Petrology, v. 42, p. 825–845, doi:10.1093/petrology/42.4.825.

Schumacher, J.C., 1991, Empirical ferric iron correction—Necessity, assumptions, and effects on selected geothermobarometers: Mineralogical Magazine, v. 55, p. 3–18, doi:10.1180/minmag.1991.055.378.02.

Thompson, R.N., and Mackenzie, W.S., 1967, Feldspar-liquid equilibria in peralkaline acid liquids—An experimental study: American Journal of Science, v. 265, p. 714–734, doi:10.2475/ajs.265.8.714.

Toplis, M.J., and Carroll, M.R., 1995, An experimental study of the influence of oxygen fugacity on Fe-Ti oxide stability, phase relations and mineral melt equilibria in ferro-basaltic systems: Journal of Petrology, v. 36, p. 1137–1170.

Watson, E.B., 1979, Zircon saturation in felsic liquids—Experimental results and applications to trace-element geochemistry: Contributions to Mineralogy and Petrology, v. 70, p. 407–419, doi:10.1007/BF00371047.

Whitaker, M., Nekvasil, H., Lindsley, D.H., and Difrancesco, N.J., 2007, The role of pressure in producing compositional diversity in intraplate basaltic magmas: Journal of Petrology, v. 48, p. 365–393, doi:10.1093/petrology/egl063.

Whitaker, M., Nekvasil, H., Lindsley, D., and McCurry, M., 2008, Can crystallization of olivine tholeiite give rise to potassic rhyolites?—An experimental investigation: Bulletin of Volcanology, v. 70, p. 417–434, doi:10.1007/s00445-007-0146-1.

White, J.C., Ren, M., and Parker, D.F., 2005, Variation in mineralogy, temperature and oxygen fugacity in a suite of strongly peralkaline lavas and tuffs, Pantelleria, Italy: Canadian Mineralogist, v. 43, p. 1331–1347, doi:10.2113/gscanmin.43.4.1331.

White, J.C., Parker, D.F., and Ren, M., 2009, The origin of trachyte and pantellerite from Pantelleria, Italy: Insights from major element, trace element, and thermodynamic modelling: Journal of Volcanology and Geothermal Research, v. 179, p. 33–55, doi:10.1016/j.jvolgeores.2008.10.007.

Wolfenden, E., Ebinger, C., Yirgu, G., Renne, P.R., and Kelley, S.P., 2005, Evolution of a volcanic rifted margin: Southern Red Sea, Ethiopia: Geological Society of America Bulletin, v. 117, p. 846–864, doi:10.1130/B25516.1.

Woolley, A.R., 2001, Alkaline Rocks and Carbonatites of the World: Part 3. Africa: Bath, UK, Geological Society of London, 372 p.

Wright, T.J., Ebinger, C.J., Biggs, J., Ayele, A., Yirgu, G., Keir, D., and Stork, A., 2006, Magma maintained rift segmentation at continental rupture in the 2005 Afar dyking episode: Nature, v. 442, p. 291–294, doi:10.1038/nature04978.

Science Editor: Nancy Riggs
Associate Editor: Calvin F. Miller

Manuscript Received 26 May 2011
Revised Manuscript Received 4 July 2012
Manuscript Accepted 16 July 2012

Printed in the USA

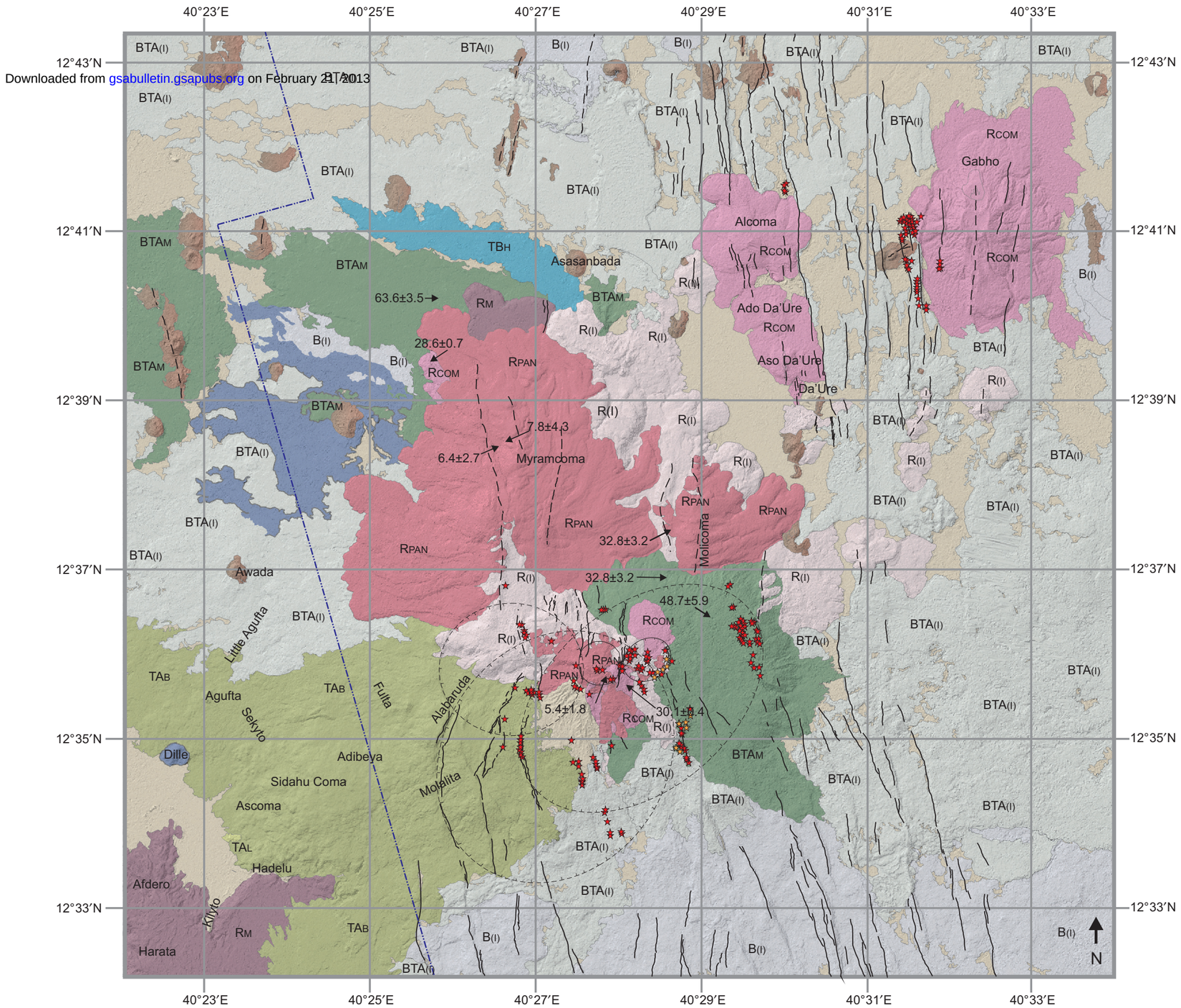

Figure 3. New geological map for Dabbahu. Units are distinguished between those that were sampled in the field and those that were interpreted from Natural Environment Research Council (UK) Airborne Research and Survey Facility (NERC ARSF) aerial photographs. Locations of samples dated by ^{40}Ar-^{39}Ar geochronology as part of this study are also shown.

List of map units

Sampled deposits

- RPAN — Pantellerite rhyolites
- RM — Metaluminous rhyolites
- RCOM — Comendite rhyolites
- Trachyte
- TAB TAL — Trachyandesite - benmoreites and latites
- BTAM — Basaltic trachyandesite - mugearites
- TBH — Trachybasalt - hawaiites
- Basalts - mildly alkaline / transitional

Inferred deposits

- R(I) — Rhyolite
- TA(I) — Trachyandesite
- BTA(I) — Basaltic trachyandesite
- TB(I) — Trachybasalt
- B(I) — Basalts

Superficial deposits

- Windblown sand, ash and pumice too thick to determine underlying bedrock

Symbols

- 33±3 — Location and age (ka) of sample determined by ^{40}Ar/^{39}Ar
- Fault
- Fissure
- Caldera (dashed line indicates inferred)
- Scoria cone
- Location of boina (active and nonactive)
- Major hydrothermal alteration
- Western limit of NERC ARSF aerial photographs

Magmatic history of Dabbahu, a composite volcano in the Afar Rift, Ethiopia
Field et al.
Figure 3
Supplement to: *Geological Society of America Bulletin*, v. 125; no. 1/2; doi:10.1130/B30560.1.S1